RESEARCH ARTICLE SUMMARY

DRUG DISCOVERY

AlphaFold2 structures guide prospective ligand discovery

Jiankun Lyu*†, Nicholas Kapolka†, Ryan Gumpper†, Assaf Alon†, Liang Wang†, Manish K. Jain, Ximena Barros-Álvarez, Kensuke Sakamoto, Yoojoong Kim, Jeffrey DiBerto, Kuglae Kim, Isabella S. Glenn, Tia A. Tummino, Sijie Huang, John J. Irwin, Olga O. Tarkhanova, Yurii Moroz, Georgios Skiniotis*, Andrew C. Kruse*, Brian K. Shoichet*, Bryan L. Roth*

INTRODUCTION: Deep-learning methods to predict protein structures, like AlphaFold2 (AF2) and RosettaFold, have had great impact on structural biology, but their influence on drug discovery is less clear. Recent retrospective docking studies suggest that AF2 models struggle to recapitulate ligand binding modes and to distinguish active from decoy molecules in ligand discovery simulations, compared with the same calculations on experimental structures. Still, these studies are retrospective; how AF2 models perform prospectively for predicting new ligands has not, to our knowledge, been explored.

RATIONALE: To address this prospective gap, we selected two therapeutic targets for which the AF2 models appeared before the experimental structures were released: the σ_2 and serotonin 2A (5-HT2A) receptors. Whereas the AF2 model resembled experimental structures overall, there were meaningful conformational differences in residues at the ligand binding sites, particularly for the 5-HT2A receptor. To prospectively test the relative ability of the AF2 models to guide the discovery of new ligands, we docked libraries of hundreds of millions to billions of molecules against both the modeled and the experimental structures, prioriti… for synthesis and testing hundreds of h… ranking molecules for each model and structure. We assessed the performance of the AF2 structures versus the experimental structures by hit rate (number experimentally active per number tested) and by hit potency.

RESULTS: Surprisingly, prospective docking against the AF2 models was as effective as it was for docking against the experimental structures. For the σ_2 receptor, 55% of the AF2-derived docking hits were active at 1 μM, whereas docking against the crystal structure led to a 51% hit rate. For the 5-HT2A receptor, 26% of the molecules from the AF2-derived model bound at 10 μM, whereas for the cryo–electron microscopy (cryo-EM) structure, 23% bound. Comparing the affinities of these hits yielded similar conclusions. Against the σ_2 receptor, the top 18 hits from the AF2 docking had inhibition constant (K_i) values between 1.6 and 84 nM, similar to the distribution from docking against the receptor crystal structure. Against the 5-HT2A receptor, the AF2 model led, if anything, to more potent and selective compounds compared with docking against the experimental structure. The most potent AF2-derived agonists had median effective concentration (EC_{50}) values ranging from 42 nM to 1.6 μM, whereas the cryo-EM–derived docking hits had EC_{50} values ranging from 246 nM to 3 μM. Three of the AF2-derived docking hits were subtype selective, whereas the cryo-EM–derived docking hits were not. A cryo-EM structure of an AF2-derived agonist bound to the 5-HT2A receptor superposed well with the docking prediction and supported several residue conformations anticipated by the AF2 model that differed from those observed in the original experimental structure.

CONCLUSION: Differences in the ligand binding sites between AF2 models and experimental structures may reduce the ability of the models to recognize known ligands. For a subset of AF2 models, however, these differences may represent low-energy, alternate receptor conformations that can guide the discovery of new ligands just as well as experimental structures can, potentially expanding the range of proteins that may be targeted for structure-based drug discovery. ■

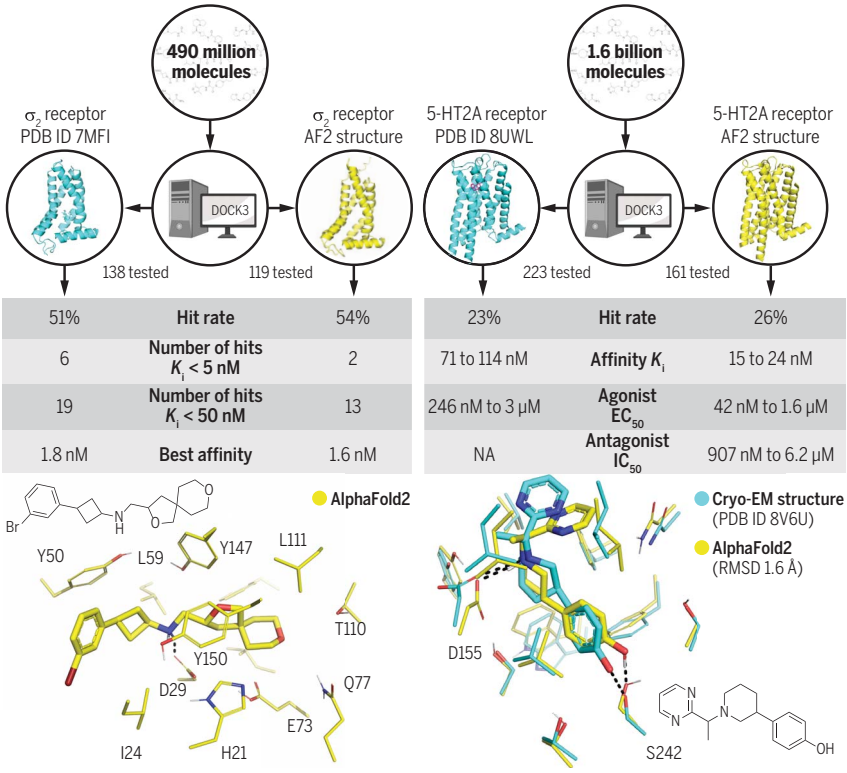

AF2 structures template prospective ligand discovery. More than 490 million and 1.6 billion molecules were docked against the AF2 and experimental structures for the σ_2 and 5-HT2A receptors, respectively. More than 100 high-ranking molecules were prioritized for synthesis and testing for each model and structure (about 500 total molecules). Judging by hit rate and hit affinity, docking against the AF2 models was as effective as docking against the experimental structures. The cryo-EM structure of the agonist Z7757 in complex with the 5-HT2A receptor superposed closely with the computational docking prediction on the AF2 model. IC_{50}, median inhibitory concentration; NA, not applicable; PDB, Protein Data Bank; RMSD, root mean square deviation. Single-letter abbreviations for the amino acid residues are as follows: D, Asp; E, Glu; H, His; I, Ile; L, Leu; Q, Gln; S, Ser; T, Thr; and Y, Tyr.

The list of author affiliations is available in the full article online.
*Corresponding author. Email: jiankunlyu@gmail.com (J.L.); yiorgo@stanford.edu (G.S.); andrew_kruse@hms.harvard.edu (A.C.K.); bshoichet@gmail.com (B.K.S.); bryan_roth@med.unc.edu (B.L.R.)
†These authors contributed equally to this work.
Cite this article as J. Lyu *et al.*, *Science* **384**, eadn6354 (2024). DOI: 10.1126/science.adn6354

READ THE FULL ARTICLE AT
https://doi.org/10.1126/science.adn6354

RESEARCH ARTICLE

DRUG DISCOVERY

AlphaFold2 structures guide prospective ligand discovery

Jiankun Lyu[1,2]*†, Nicholas Kapolka[3]†, Ryan Gumpper[3]†, Assaf Alon[4]†‡, Liang Wang[5]†, Manish K. Jain[3], Ximena Barros-Álvarez[5], Kensuke Sakamoto[3,6], Yoojoong Kim[3], Jeffrey DiBerto[3]§, Kuglae Kim[3]¶, Isabella S. Glenn[1], Tia A. Tummino[1], Sijie Huang[1], John J. Irwin[1], Olga O. Tarkhanova[7], Yurii Moroz[7,8,9], Georgios Skiniotis[5,10]*, Andrew C. Kruse[4]*, Brian K. Shoichet[1]*, Bryan L. Roth[3,6,11]*

AlphaFold2 (AF2) models have had wide impact but mixed success in retrospective ligand recognition. We prospectively docked large libraries against unrefined AF2 models of the σ_2 and serotonin 2A (5-HT2A) receptors, testing hundreds of new molecules and comparing results with those obtained from docking against the experimental structures. Hit rates were high and similar for the experimental and AF2 structures, as were affinities. Success in docking against the AF2 models was achieved despite differences between orthosteric residue conformations in the AF2 models and the experimental structures. Determination of the cryo–electron microscopy structure for one of the more potent 5-HT2A ligands from the AF2 docking revealed residue accommodations that resembled the AF2 prediction. AF2 models may sample conformations that differ from experimental structures but remain low energy and relevant for ligand discovery, extending the domain of structure-based drug design.

Structure-based library docking is widely used in early ligand discovery (*1*); on targets with well-formed binding sites (*2*, *3*), the affinities of direct docking hits can reach the mid-nanomolar or even high picomolar range (*4*–*13*). These docking campaigns have mostly relied on experimental protein structures from crystallography or, more recently, cryo–electron microscopy (cryo-EM), but for many drug targets (*14*), such experimental structures remain unavailable. In these cases, homology models have been used (*15*–*17*). These models show promise, particularly when the sequence identity between the target and template exceeds 50% (*18*). Many targets are outside of this range, and docking against homology models is often thought to reduce performance relative to docking against experimental structures.

Recent breakthroughs in protein structure predictions, led by deep-learning methods such as AlphaFold2 (AF2) (*19*) and RosettaFold (*20*), promise to overcome this limitation. AF2 has demonstrated an unprecedented ability to predict protein structures with atomic accuracy (*19*) and operates at scale (*21*, *22*). As of this writing, the AlphaFold database features protein structures for the human proteome and for those of 47 other organisms, covering more than 200 million proteins and nearly all potential therapeutic protein targets. These structures have proven very useful for applications in structural biology (*23*–*25*), protein design (*26*, *27*), protein-protein interaction (*28*–*30*), target prediction (*31*, *32*), protein function prediction (*33*, *34*), and biological mechanism of action (*35*–*37*).

The impact of AF2 structures on structure-based ligand discovery has been murkier. Although the global accuracy of the models has been impressive, concerns have arisen regarding their accuracy in modeling ligand binding sites (*38*), where high fidelity to low-energy conformations is thought to be crucial, and small errors, relatively unimportant for other applications, can disrupt ligand recognition and pose prediction. Indeed, retrospective studies have suggested that docking against unrefined AF2 models struggles to recognize and pose known ligands compared with decoy molecules and performs better against experimental structures in equivalent comparisons (*7*, *39*–*48*). A drawback to these studies is that they are biased by the past; that is, known ligands can affect the conformations adopted by experimental structures when they are determined in complex with them, whereas experimental structures can influence the exploration of new ligands. Thus, it is possible that the relatively poor performance of AF2 models in retrospective simulation of structure-based ligand discovery may underestimate the ability of AF2 structures to template new ligand discovery prospectively. To test this idea, we docked identical ultralarge libraries against the unrefined AF2 models of the σ_2 and serotonin 2A (5-HT2A) receptors and against experimental structures of these two receptors. Hundreds of molecules that were highly ranked by docking were synthesized against each of the four structures, and hit rates and ligand affinities were compared.

Results

Assessing AF2 predictions

For the σ_2 and 5-HT2A receptors, AF2 models had been predicted before the crystal structures were released, reducing possible bias. These two receptors belong to two unrelated protein families, the EXPERA and G protein–coupled receptors (GPCRs), respectively. In both models, AF2 predicted uncollapsed binding sites, unlike several other targets where we judged the AF2-predicted binding sites to be too compressed to support ligand fitting (fig. S1). For instance, superposition of an experimental ligand-receptor complex on the AF2 model of the MRGPRX4 receptor resulted in 4 of 26 ligand atoms clashing with the surface of the modeled receptor, reflecting the collapse of the orthosteric site in the model. For the σ_2 receptor, the AF2 structure recapitulated the side-chain conformations of all orthosteric site residues to 1.1-Å root mean square deviation (RMSD) versus the crystal structure, with few residues with individual RMSD values greater than 1.5 Å (Fig. 1). For the 5-HT2A receptor, although most binding site residues were well predicted (RMSD <2 Å versus the cryo-EM structure), two residues differed by 2.5- to 3.1-Å RMSD, adopting different rotamers (Fig. 1). Both the experimental structures and the AF2 models of the σ_2 and 5-HT2A receptors had sites that were judged ligandable by the widely used SiteMap program (*49*) (scores were 1.3 and 1.2 for the σ_2 crystal structure and AF2 model orthosteric sites, respectively, and 1.2 for both the cryo-EM and AF2 structures of the 5-HT2A receptor orthosteric site; numbers >1 are favorable for ligand binding). Thus, the σ_2 and 5-HT2A receptors occupy two of what are perhaps three categories of AF2 models for ligand discovery: (i) those that are close to the experimental ligand binding site but still harbor meaningful side-chain differences, (ii) those that are overall close but have several residues

[1]Department of Pharmaceutical Chemistry, University of California, San Francisco, CA 94158, USA. [2]The Evnin Family Laboratory of Computational Molecular Discovery, The Rockefeller University, New York, NY 10065, USA. [3]Department of Pharmacology, University of North Carolina at Chapel Hill School of Medicine, Chapel Hill, NC 27599, USA. [4]Department of Biological Chemistry and Molecular Pharmacology, Blavatnik Institute, Harvard Medical School, Boston, MA 02115, USA. [5]Department of Molecular and Cellular Physiology, Stanford University School of Medicine, Stanford, CA 94035, USA. [6]National Institute of Mental Health Psychoactive Drug Screening Program (NIMH PDSP), School of Medicine, University of North Carolina at Chapel Hill School of Medicine, Chapel Hill, NC 27599, USA. [7]Chemspace LLC, Kyiv 02094, Ukraine. [8]Taras Shevchenko National University of Kyiv, Kyiv 01601, Ukraine. [9]Enamine Ltd., Kyiv 02094, Ukraine. [10]Department of Structural Biology, Stanford University School of Medicine, Stanford, CA 94304, USA. [11]Division of Chemical Biology and Medicinal Chemistry, Eshelman School of Pharmacy, University of North Carolina at Chapel Hill, Chapel Hill, NC 27599, USA.

***Corresponding author. Email: jiankunlyu@gmail.com (J.L.); yiorgo@stanford.edu (G.S.); andrew_kruse@hms.harvard.edu (A.C.K.); bshoichet@gmail.com (B.K.S.); bryan_roth@med.unc.edu (B.L.R.)**

†These authors contributed equally to this work.

‡Present address: Pharmacology Department, Yale School of Medicine, New Haven, CT 06510, USA.

§Present address: EvE Bio LLC, Durham, NC 27703, USA.

¶Present address: Department of Pharmacy, College of Pharmacy, Yonsei University, Incheon 21983, Korea.

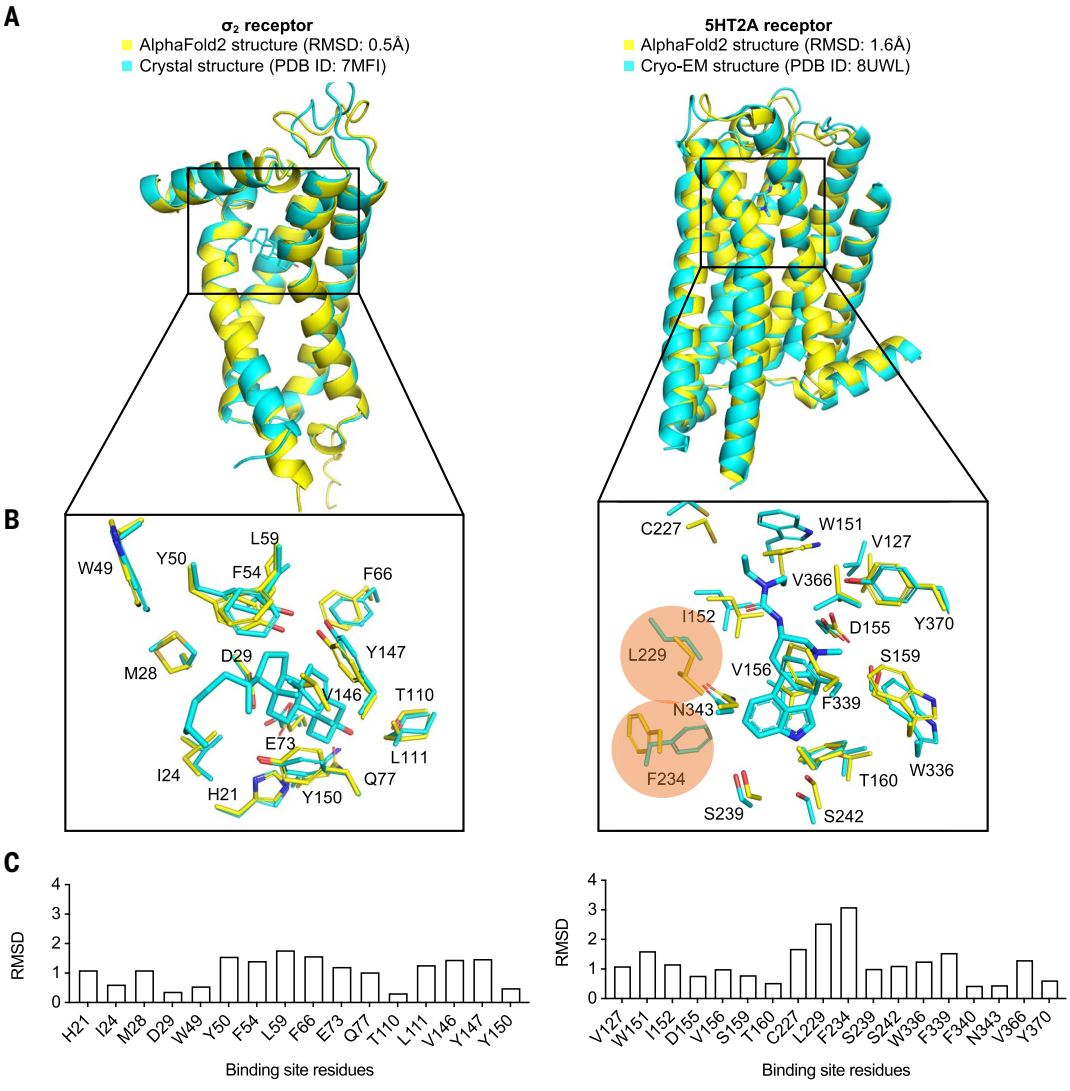

Fig. 1. Structural comparisons of the AF2 predicted structure and experimental structure for the σ_2 and 5-HT2A receptors. The σ_2 receptor is shown in the left column and the 5-HT2A receptor in the right column. (**A** and **B**) The experimental structure (*7*) (cyan) is overlaid with the AF2 predicted structure (yellow). The RMSD values were calculated based on backbone atoms. The ligand binding site residues were selected within a 5-Å distance from the ligand. In (B), two residues with large conformational differences between the AF2 and experimental structures used in docking, L229 and F234, are highlighted in orange for the 5-HT2A receptor. (**C**) The full-atom RMSD values of the binding site residues between the AF2 and the experimental structures. Single-letter abbreviations used in the figures for the amino acid residues are as follows: C, Cys; D, Asp; E, Glu; F, Phe; G, Gly; H, His; I, Ile; L, Leu; M, Met; N, Asn; Q, Gln; S, Ser; T, Thr; V, Val; W, Trp; and Y, Tyr.

in substantially different conformations, and (iii) those for which the modeled sites differ so much from the experimental sites as to preclude ligand recognition without extensive refinement (fig. S1).

Retrospective docking of known ligands against the AF2 structures

We began by docking known ligands against the AF2 models of the σ_2 and 5-HT2A receptors using DOCK3.8 (*50*, *51*), which samples flexible ligands in millions of poses, scoring each for physical fit to a predefined site, which is typically kept rigid. In DOCK3.8, ligand-protein fit is evaluated by calculating both electrostatic interactions using a probe-charge model of the Poisson-Boltzmann equation (*51*, *52*) and van der Waals interactions by adapting the AMBER potential function (*52*) and then correcting these terms for ligand desolvation (*50*, *53*) and for ligand conformational strain (*54*). Other docking programs often model similar energy terms (*55*–*58*).

Our approach to these retrospective calculations took two forms: (i) taking ligands found from our previous docking campaigns against the experimental structures of the two receptors and redocking them against the AF2 models and (ii) docking previously known ligands from the general literature (which do not include the docking-derived ligands). Against the crystal structure of the σ_2 receptor, we had previously screened (*7*) 490 million make-on-demand ("tangible") molecules from the ZINC20 library of dockable molecules (*59*). From among the top-ranking 300,000 molecules (top 0.06% of the ranked library), we tested 138 high-scoring ones by radioligand competition, of which 70 displaced more than 50% of the known ligand [^{3}H]-DTG at 1 μM, a hit rate of 51% (*7*) (Fig. 2A, left). The best 21 actives had inhibition constant (K_i) values between 1.8 nM and the low-μM range, with 19 having K_i values <50 nM and six having K_i values <5 nM (*7*) (Fig. 2B). When we redocked the same 490 million–molecule library against the AF2 model of σ_2, the ranks of these same 138 formerly high-ranking molecules dropped so far that they were no longer among the top 300,000. This may reflect the slight shrinking of the AF2 orthosteric site compared with the crystal structure orthosteric site, which dropped to a calculated (*49*) 213 from 268 Å^3, respectively. Correspondingly, when docking known σ_2 ligands from the ChEMBL database versus a library of property-matched decoys—a widely used control in docking—the crystal structure (logAUC of 39; AUC, area under the curve) returned much higher enrichments than did the AF2 model (logAUC of 16; fig. S2A). Related retrospective studies against the cryo-EM and AF2 structures of the 5-HT2A receptor had similar results: The experimental structure led to higher retrospective enrichment of 41 known ligands over property-matched decoys for the experimental structure than it did for the AF2 structure (fig. S2B). These observations are consistent with previous retrospective studies that

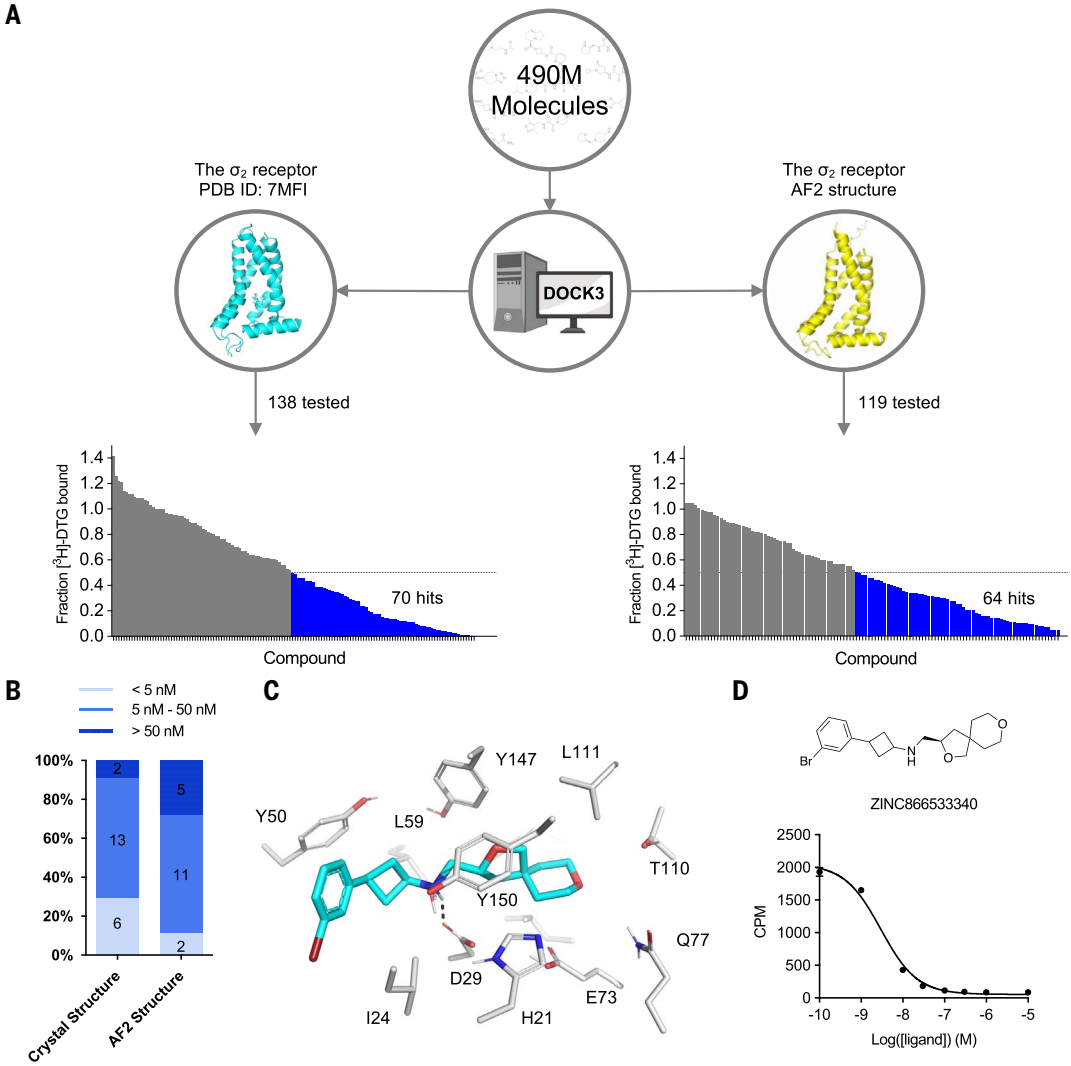

Fig. 2. Comparison of prospective screens against the crystal and AF2 structures of the σ_2 receptor. (**A**) The same 490 million molecules from ZINC20 were screened against both the crystal and AF2 structures of the σ_2 receptor. From these, 138 molecules from the crystal docking campaign and 119 from the AF2 docking campaign were synthesized and tested in a radioligand displacement assay. The campaign involving the crystal structure has already been published. The data shown on the left were replotted based on the previously published dataset. Displacement of the radioligand [^{3}H]-DTG by each tested molecule occurs at 1 μM (mean ± SEM of three technical replicates). The horizontal dashed lines indicate 50% radioligand displacement. Bars below the dashed lines represent confirmed binders, which are colored in blue. (**B**) The distribution of binding affinity levels among the hits from both the AF2 and crystal structure screens. We measured competition binding curves for the top 21 docking hits from the crystal structure screen and the top 18 hits from the AF2 structure screen. These hits are categorized into three affinity ranges: <5 nM, 5 to 50 nM, and >50 nM. (**C**) The docked poses of the best binder from the screen against the AF2 model. (**D**) The competition binding curve of the best binder from (C) against the σ_2 receptor. The data are represented as mean ± SEM from three technical replicates. Mean values and standard error are available in data S1.

compared AF2 models with experimental structures for ligand discovery (*7*, *39*–*48*).

Prospective docking against the σ_2 AF2 structure

A potential flaw in the retrospective logic is that the ligands chosen are biased by the receptor structure, and the receptor conformation is adapted to the ligands with which it was determined. For instance, the 70 new ligands that emerged from docking against the crystal structure of σ_2 (*7*) fit that structure better than the AF2 model, and even ChEMBL ligands share this bias of the known. Indeed, both the experimental structures and the AF2 models of the σ_2 and 5-HT2A receptors had sites that were judged ligandable by SiteMap (*49*) (scores were 1.3 and 1.2 for the σ_2 crystal structure and AF2 model orthosteric sites, respectively, and 1.2 for both the cryo-EM and AF2 structures of the 5-HT2A receptor orthosteric site; numbers >1 are favorable for ligand binding). A second potential flaw is that these retrospective control calculations are limited to the chemotypes of the known ligands and do not necessarily predict outcomes for new chemotypes explored in an unbiased large library. Thus, it is conceivable that even though the AF2 structures are worse at recapitulating known actives, they might still prioritize new ligands from large-library docking.

To investigate this possibility, we docked the same 490 million–molecule tangible library against the σ_2 receptor's AF2 model (as mentioned above), selecting 119 new molecules from the top 300,000 docked for synthesis and testing (table S1). Of these, 64 molecules displaced over 50% [^{3}H]-DTG–specific σ_2 binding at 1 μM, a hit rate of 54%. Although slightly higher than the 51% observed in the crystal structure docking campaign, the two hit rates were not significantly different based on a z-test. The top 18 hits from the AF2 campaign had K_i values between 1.6 and 84 nM, with 13 having K_i values <50 nM and two with K_i values <5 nM (Fig. 2B and fig. S3). Although the highest affinity is comparable between the screens for the crystal and AF2 structures, the affinity distribution is slightly better for the crystal structure campaign. Intriguingly, despite the similarities in hit rates and affinity ranges, only one of the 134 new ligands shared even the same core scaffold between the crystal structure and AF2 campaigns (fig. S4), and none of the ligands between the two campaigns were the same. By ECFP4-based Tanimoto coefficient (Tc) analysis, the two sets of experimentally confirmed ligands have an average Tc of 0.32, not far from random for this fingerprint. Consistent with the diversity, the most potent ligand from the AF2 campaign, ZINC866533340 (K_i of 1.6 nM), represented a chemotype previously unseen for the σ_2 receptor (Fig. 2, C and D).

As an aside, although all molecules tested against the σ_2 AF2 model ranked among the top 0.06% of the docked library, about half of those prioritized were human-picked from among this pool, and about half were simply picked by dock score, as was true for the campaign against the crystal structure (*7*) (see Materials and methods). In docking against the AF2 model, hit rates for high-ranking molecules prioritized both by score and by human selection were not statistically different from those picked simply by rank order. We do note that the three hits with K_i values better (lower) than 10 nM were from human prioritization (fig. S3), but whether this is significant or not is uncertain because we only determined full K_i values for 18 molecules overall, and most AF2-derived and crystal structure–derived ligands were interleaved by K_i.

Prospective docking against 5-HT2A experimental receptor structure and the AF2 model

We further investigated using AF2 structures for prospective ligand discovery by targeting the 5-HT2A receptor, a widely studied drug target for depression and for psychedelic experience (*60*). Here, the AF2 model presented potentially greater challenges for docking than the AF2 model of the σ_2 receptor, with larger binding-site conformational differences. As with the σ_2 receptor, we compared prospective docking success against the AF2 model with that of an experimental structure. For the latter, we used the complex of the 5-HT2A receptor with the partial agonist lisuride and with mini Gαq (fig. S5). Lisuride is a potent and nonpsychedelic partial agonist, and its structure seemed suited to longstanding efforts to discover previously unknown nonpsychedelic 5-HT2A agonists (*61*). Because the structure of the lisuride–5-HT2A–mini-Gαq structure has not been previously described, we briefly do so here.

To isolate an active-state heterotrimeric complex, we used a mini-GαqiN–Gβ1–Gγ2 heterotrimer coexpression system in the presence of stabilizing single-chain antibody scFv16 (*62*). Each component was purified separately, and the active-state complex was formed in the presence of lisuride. We subjected this complex to single-particle cryo-EM analysis and built a consensus reconstruction at 3.1 Å through multiple steps of three-dimensional (3D) classification and focused refinement (fig. S5). The definition of the cryo-EM density allowed us to unambiguously model lisuride within the orthosteric pocket (table S2) with the binding pose validated by Gemspot (*63*). The global structural features were consistent with previous 5-HT2A ternary complex cryo-EM reconstructions and with other receptor-Gαq–bound structures (*64*–*67*). In this active-state structure, lisuride recapitulates many interactions seen in an inactive-state crystallographic complex (*68*) [Protein Data Bank (PDB) ID 7WC7], with some important differences. As in the crystal structure, lisuride's indole hydrogen-bonds with S242$^{5.46}$, its cationic nitrogen ion-pairs with D155$^{3.32}$, and its diethylamide packs with W151$^{3.28}$ (fig. S6) [superscripts use Ballesteros-Weinstein and GPCRdb (*69*) nomenclature (*70*); S, D, and W indicate Ser, Asp, and Trp, respectively].

Unlike the case with the σ_2 receptor, the AF2 model of the 5-HT2A receptor exhibited notable rotamer changes in several orthosteric site residues compared with the cryo-EM structure. Overall, the backbone RMSD between modeled and experimental structures was 1.6 Å (compared with 0.5 Å for σ_2). Although most orthosteric residues had an RMSD <1.5 Å, key residues F234$^{5.38}$ on transmembrane helix 5 (TM5) and L229$^{45.52}$ on the extracellular loop 2 (ECL2) loop differed by 2.5 and 3.1 Å, respectively, adopting different rotamers in the two structures (Fig. 1, right) (F, Phe; L, Leu). Also, W151$^{3.28}$ is pushed outward in the lisuride cryo-EM structure (PDB ID 8UWL) versus the AF2 model, owing to packing with the ligand's diethylamide. These differences shrink the orthosteric pocket in the AF2 model compared with that of the lisruide cryo-EM structure used in the docking, from 816 Å^3 in the experimental structure to 732 Å^3 in the AF2 model. Because the AF2 model draws on sequence similarity from an overall family of related 5-HT receptors, and because the cryo-EM structure represents an active state of the receptor in complex with Gαq, whereas the AF2 model more closely resembles an inactive state (fig. S7), we anticipated that the experimental structure would be more likely to select agonists that are 5-HT2A selective and Gαq biased. However, both docking campaigns targeted residues key for agonist recognition, key for bias, and key for subtype selectivity (*71*) (S239, S242, T160, F234, and F339; T, Thr). In this sense, both docking campaigns were biased toward finding 5-HT2A agonists.

More than 1.6 billion tangible molecules were docked against both the cryo-EM and AF2 receptor structures, again using DOCK3.8. We considered the top 3 million (top 0.2%) molecules from docking against each structure, applying consistent filtering, clustering, and hit-picking criteria for both structures to reduce these to a set of prioritized molecules for synthesis and testing (e.g., we only picked molecules topologically unrelated to known 5-HT2A ligands, we insisted that the molecules picked were topologically diverse among themselves, and we excluded molecules that buried uncompensated hydrogen-bond donors; see Materials and methods). Ultimately, 223 high-ranking molecules docked against the cryo-EM structure and 161 high-ranking molecules docked against the AF2 structure were synthesized (table S3).

In primary radioligand binding screening assays, 51 of the 223 molecules from docking against the cryo-EM structure displaced more than 50% [^{3}H]–lysergic acid diethylamide ([^{3}H]-LSD) at 10 μM of the docked ligand (Fig. 3, A and B, left), a hit rate of 23%. Meanwhile, 42 of the 161 molecules from docking against the AF2 model met this threshold, a hit rate of 26% (Fig. 3, A and B, right). Applying a stricter criterion, where displacement greater than 90% [^{3}H]-LSD at 10 μM defines a potentially potent hit, the rates were 4% (eight hits per 223 tested) and 6% (nine hits per 161 tested) for docking against the cryo-EM and the AF2 structures, respectively. In secondary radioligand binding assays, these top 17 hits had K_i values between 15 and 344 nM (fig. S8 and table S4). Unexpectedly, the three compounds with the highest affinities (15 to 24 nM) were all from the AF2 docking campaign, whereas the three best compounds from the cryo-EM docking campaign displayed affinities about fivefold weaker (between 71 and 114 nM) (fig. S8 and table S4). Although the AF2 docking hit rates are higher, they do not differ significantly from the experimental docking hit rates based on a z-test. Meanwhile, of the 93 active molecules from both campaigns, no two shared the even same scaffold (fig. S4, bottom), and the Tc average pairwise similarity was 0.27, close to random.

We next screened the 338 docking-prioritized molecules from both campaigns for functional activity (i.e., agonism or antagonism); for subtype selectivity among the 5-HT2A, 5-HT2B, and 5-HT2C receptors; and for ligand bias for either Gαq activation or β-arrestin2 recruitment. Because of the large number of compounds, this was initially done at a single concentration and then subsequently in full concentration-response results for the more interesting compounds. After treatment with 3 μM of each compound, 10 compounds from the cryo-EM docking set and six from the AF2 docking set emerged as 5-HT2A agonists, defined by ≥10% 5-HT response (Fig. 3C). We also observed 10 compounds (five cryo-EM and five AF2) and six compounds (three cryo-EM and three AF2) that were 5-HT2B and 5-HT2C agonists (fig. S9). When screened for antagonist activity at 3 μM, five compounds (one cryo-EM and four AF2) antagonized 5-HT2A receptor activity, as defined by ≥20% clozapine activity (Fig. 3D). Additionally, we found 17 compounds (10 cryo-EM and seven AF2) and one compound (cryo-EM) with antagonist activity at the 5-HT2B and 5-HT2C receptors, respectively (fig. S9). Comparisons of our primary binding data (Fig. 3B) with our functional screening data (Fig. 3, C and D) indicate that two of the top 17 binding hits exhibit 5-HT2A agonist activity (fig. S8 and table S4), whereas 15 antagonize 5-HT2A activity. Notably, both of the high-affinity agonists (Z2504 and Q2118) were from the AF2 dataset.

Dose-response curves measuring calcium mobilization confirmed 5-HT2A agonist activity of the top hits from both the cryo-EM and

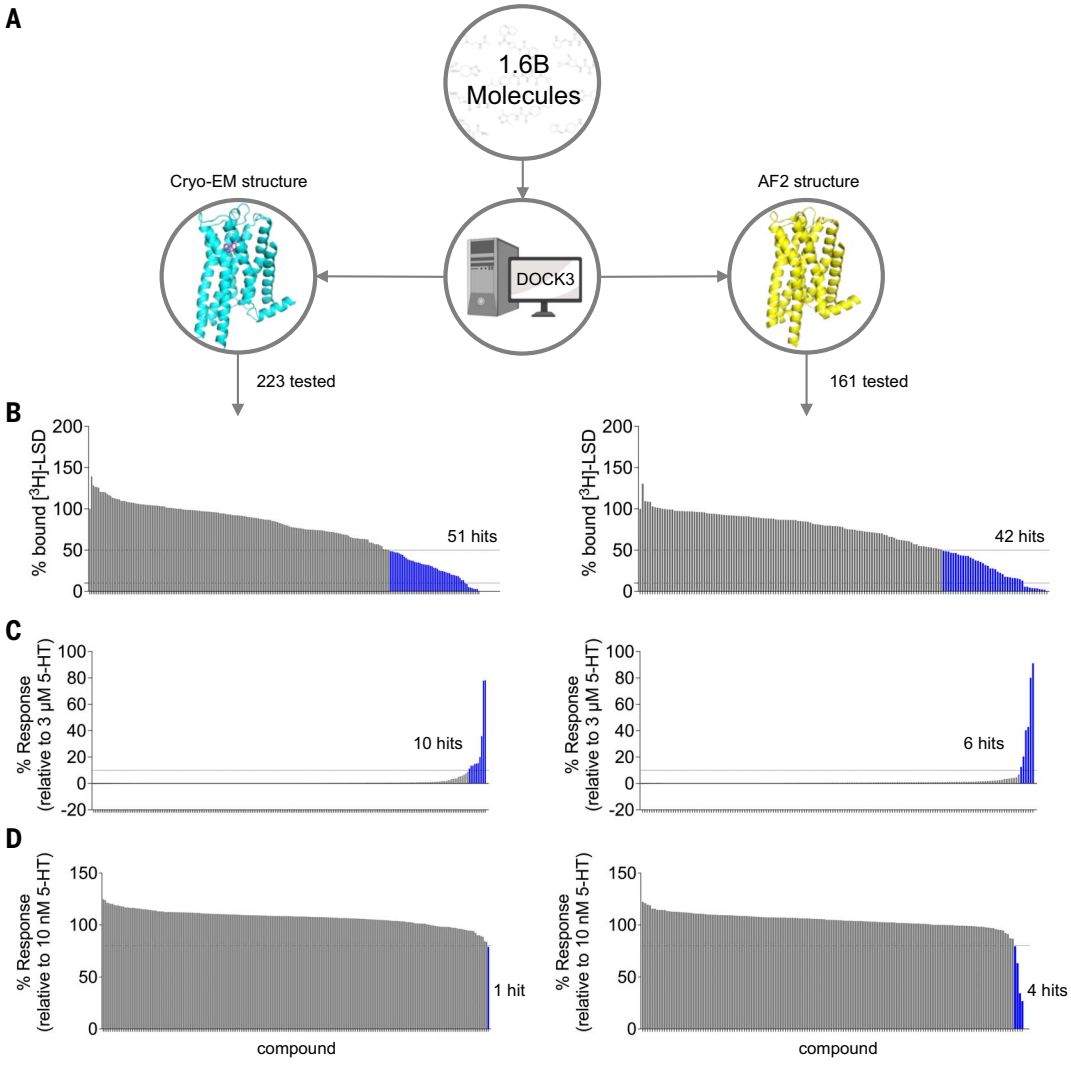

Fig. 3. Comparison of prospective screens against the cryo-EM and AF2 structures of the 5-HT2A receptor. (**A**) The same set of 1.6 billion molecules from ZINC22 were docked against the cryo-EM and AF2 structures of the 5-HT2A receptor. Of these, 223 molecules were prioritized from the cryo-EM docking campaign (left) and 161 from the AF2 docking campaign (right). (**B**) Displacement of the radioligand [^{3}H]-LSD by each molecule at 10 μM (mean ± SEM of three independent replicates). The horizontal dashed lines indicate 50 and 90% radioligand displacement, respectively. (**C**) The Ca^{2+} mobilization functional assay in agonist mode. Each compound was tested at a concentration of 3 μM. the horizontal dashed lines indicate agonism equivalent to 10% 5-HT activity. Data are presented as mean ± SEM from three biological replicates. (**D**) The Ca^{2+} mobilization functional assay in antagonist mode. Each compound was tested at a concentration of 3 μM. The dashed lines indicate antagonism equivalent to 20% clozapine activity. Data are presented as mean ± SEM from three biological replicates. Mean values and standard error are available in data S2.

AF2 docking sets (Fig. 4, A and B, top). The potencies [negative logarithm of the median effective concentration (pEC_{50}) values] of top agonists from the cryo-EM docking set ranged from 246 nM to 3 μM, whereas those from the AF2 docking set ranged from 42 nM to 1.6 μM (Fig. 4 and table S5). Three of the top five AF2 agonists (Q2118, Z7757, and Z2504) displayed subtype selectivity for the 5-HT2A receptor over the 5-HT2B and 5-HT2C receptors (Fig. 4B). Meanwhile, none of the top cryo-EM agonists displayed 5-HT2A receptor selectivity. Thus, in full-concentration response, it was the AF2-derived agonists that emerged as the most potent and selective molecules.

In bioluminescence resonance energy transfer (BRET) experiments measuring heterotrimeric Gαq protein dissociation, which reflects G protein activation (*72*) versus β-arrestin2 recruitment (fig. S10 and table S5), nine of the top 10 agonists from both docking sets exhibited modest bias toward Gαq signaling versus 5-HT, whereas only one compound showed modest bias toward β-arrestin2 recruitment at high concentrations. Similar experiments with the top antagonist hits identified from primary (fig. S9) and functional screening (fig. S11) confirmed weak inhibition of 5-HT2A receptor activity, where the potencies of antagonists from the cryo-EM docking set were between 13 and 78 μM, whereas those from the AF2 docking set were between 907 nM and 114 μM (fig. S12 and table S6).

Controls for nonspecific binding

One reason why the hit rates for docking against the AF2 models and the experimental structures might resemble each other is if many of the actives are promiscuous and artifactual. To control for this, 36 of the more potent ligands from all four campaigns were counter-screened against an unrelated GPCR, the V1A vasopression receptor; none of them were active as either agonists or antagonists (fig. S9). Of these 36 molecules, 30 were also tested for colloidal aggregation, perhaps the single-most-common mechanism for promiscuous activity (*73*, *74*). This was done by measuring particle formation by dynamic light scattering (DLS) and by measuring inhibition of the counter-screen enzyme malate dehydrogenase (MDH). At 31.6 μM, typically more than 10-fold higher than their on-target activities, none of the 30 formed particles by DLS (fig. S13, B and C) nor did any substantially inhibit the widely used counter-screening enzyme MDH (fig. S13A), which is inconsistent with a colloidal mechanism of action. These results support a non-promiscuous mechanism of action for at least the more potent of the ligands found in these studies, though naturally they do not prove it.

Cryo-EM structure of an AF2-derived ligand bound to the 5-HT2A receptor

To investigate the molecular basis of recognition for agonists found by docking against the AF2 model, we determined a new cryo-EM

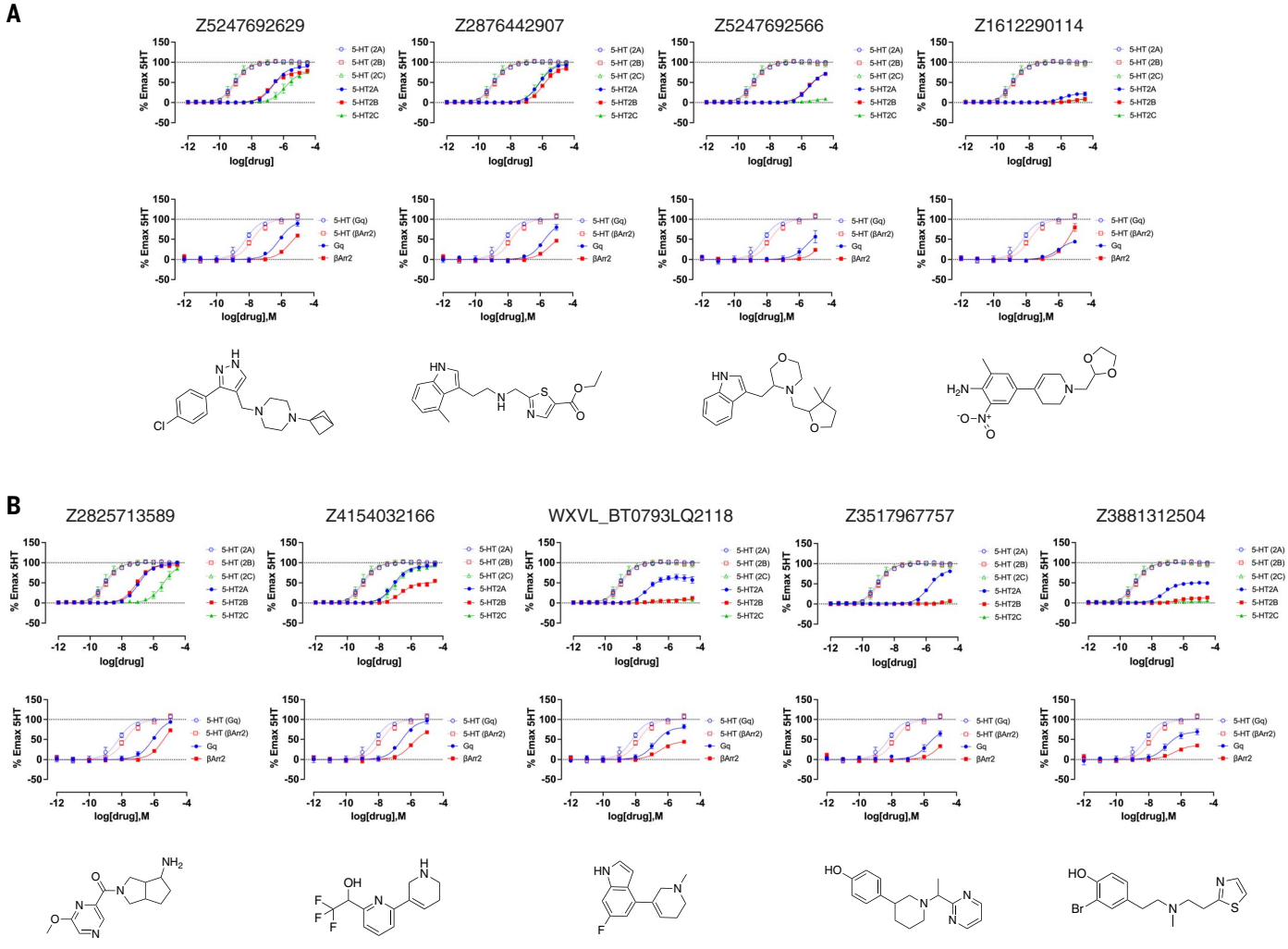

Fig. 4. Dose-response curves of the top agonists against the 5-HT2A, 5-HT2B, and 5-HT2C receptors. Top agonists from both docking campaigns were tested at the 5-HT2A (blue), 5-HT2B (red), and 5-HT2C (green) receptors. (**A**) Data from functional assays measuring calcium mobilization (top) and Gαq protein dissociation or β-arrestin2 recruitment (bottom) for the top four agonists from the cryo-EM docking campaign. Fit parameters for each compound can be found in table S5. (**B**) Data from functional assays measuring calcium mobilization (top) and Gαq protein dissociation or β-arrestin2 recruitment (bottom) for the top five agonists from the AF2 docking campaign. For (A) and (B), the chemical structure of each compound is displayed below its respective dose-response curve. Data are presented as mean ± SEM from three biological replicates.

structure with one of the selective agonists from the AF2 screen, Z7757, bound to the receptor in complex with mini-Gαq (Fig. 5B). This molecule had little topological similarity to the 5-HT2A receptor agonists of which we are aware. The 5-HT2A receptor was coexpressed with mini-GαqiN–Gβ1–Gγ2 heterotrimer and purified in the presence of Z7757 and of scFv16, as previously described (*66*, *75*, *76*). This permitted direct isolation of the complex, and a single size-exclusion step afforded us a large amount of complex for grid preparation. Purified complexes were subjected to single-particle cryo-EM analysis (fig. S14), during which particles that did not contain scFv16 were filtered out by 2D-3D classification and a focused no-alignment 3D classification and refinement on the receptor was carried out. The structure was determined to a global resolution of 3.0 Å, allowing us to unambiguously build Z7757 within the orthosteric pocket (Fig. 5B). We further validated the binding pose with Emerald (fig. S15), which uses a genetic algorithm to fit the ligand using the cryo-EM density map as restraints (*77*). The Cα-RMSD of the receptor was close to that of the active-state lisuride structure (0.78 Å) and recapitulated the receptor-Gαq interactions in prior 5-HT2A receptor structures (*60*, *61*, *66*, *75*) (Fig. 5C).

The binding of Z7757 to 5-HT2A in the new cryo-EM structure resembles the pose predicted by docking. As anticipated in the docked model, Z7757 interacts with key recognition and activation residues (Fig. 5, D to F), and the docked pose of Z7757 superposes on the experimental result with an RMSD of 1.6 Å. The major difference between the two poses comes from a 44° rotation of the agonist's distal pyrimidine ring (Fig. 5G). In both the docking prediction and the cryo-EM structure, the new agonist uses its phenolic hydroxyl to hydrogen-bond with well-known activation residues on TM3 and TM5 ($T160^{3.37}$ and $S242^{5.46}$) and also with the backbone of $G238^{5.42}$ (G, Gly), an interaction predicted in the docking but unusual among 5-HT2A receptor agonists. As expected, the cationic nitrogen of Z7757 ion-pairs with the key recognition $D155^{3.32}$ of 5-HT2A, whereas the molecule overall packs well with the binding sites in both the modeled and experimental structures.

Stepping back from the local interactions between Z7757 and receptor, it was interesting to consider how the AF2 model compares with the new cryo-EM structure in regions where we expected important differences. Orthosteric site residues $L229^{45.52}$, $F234^{5.38}$, and $W151^{3.28}$ adopt different positions and even rotamers in the AF2 model compared with the cryo-EM active-state structure against which we docked as the experimental structure, with residue

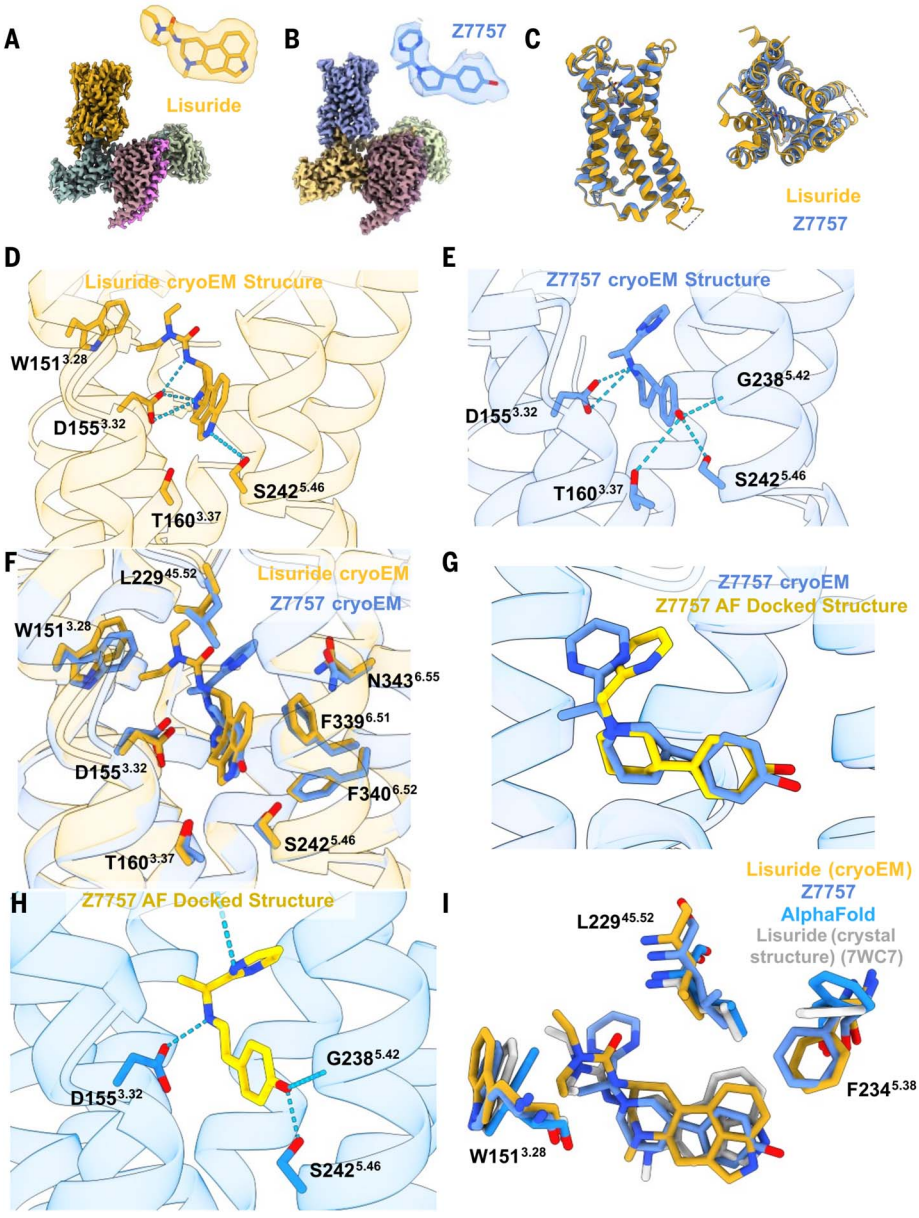

Fig. 5. Structural characterization of the 5-HT2A receptor in complex with lisuride and Z7757. (**A** and **B**) Maps of lisuride (A) and Z7757 (B) active-state heterotrimers. Models of the compounds built into the electron density are shown. (**C**) Overlay of the lisuride and Z7757 structures, which superpose to 0.78-Å Cα-RMSD. (**D** and **E**) Interactions between lisuride and the receptor (D) and between Z7757 and the receptor (E). (**F**) Overlay of Z7757 and lisuride in the orthosteric pocket. (**G**) Comparison of the experimental Z7757 structure and the predicted structure from the AF2 docking screen. (**H**) Predicted interactions from the docked pose of Z7757 in the AF2 structure. (**I**) Aligned lisuride cryo-EM structure, AF2-model, Z7757 cryo-EM structure, and the lisuride crystal structure (PDB ID 7WC7) highlighting residues that showed the biggest difference between the AF2 model and lisuride cryo-EM structures and that were used in the docking studies. In (D), (E), and (H), dashed lines indicate potential modeled interactions between the ligand and the receptor.

RMSD values of 2.5, 3.1, and 1.6 Å, respectively. The rotamer of F234$^{5.38}$ in the new Z7757-bound cryo-EM structure closely resembles that in the lisuride-bound cryo-EM structure against which we docked (Fig. 5I). Although this is a rotamer that the AF2 model failed to anticipate, F234$^{5.38}$ is distant from the new agonist in the Z7757 complex, with their closest approach being 5.9 Å, reducing the impact of this residue on recognition. Intriguingly, the overall position of L229$^{45.52}$ in the Z7757 complex more closely resembles its position in the AF2 model, which we docked against to find Z7757, than its position in the cryo-EM of the lisuride–5-HT2A structure, which we used in the experimental docking screen (Fig. 5I). Finally, W151$^{3.28}$ in the Z7757 complex more closely resembles the lisuride cryo-EM structure used in the experimental structure docking than the AF2 model. Nevertheless, W151$^{3.28}$ has still swung inward versus its position in the lisuride–5-HT2A cryo-EM (experimental) structure used for docking—in the AF2 model, this pocket-constricting rotation is further exaggerated. The constriction of this part of the orthosteric site reduces the complementarity of LSD-like ligands, including lisuride and many others characterized for the 5-HT2A receptor while still allowing the pyrimidine of Z7757 to fit well (Fig. 5I). Indeed, among the 5-HT2A structures deposited in the PDB, W151$^{3.28}$ adopts a range of conformations, opening and closing this part of the site, with the active-state lisuride complex adopting the most open position of the set (fig. S16, A to C). Meanwhile, both a non-classical agonist (*R*-69, PDB ID 7RAN) (fig. S16B) and an antagonist (zotepine, PDB ID 6A94) exhibited rotamers of W151$^{3.28}$ that resemble the rotamer adopted in the AF2 model (fig. S16C). We also found that all of the crystal structure ligand complexes with the 5-HT2A receptor, except the complex with LSD (PDB ID 6WGT), have F234$^{5.38}$ in a conformation akin to that of the AF2 models used for the docking, whereas the cryo-EM structures have consistently exhibited the altered orientation (fig. S16A). Taken together, these observations support the idea that the AF2 model sampled low-energy states of these residues, even though they differ from the particular conformations seen in the structure that was used for the second 5-HT2A receptor docking campaign (i.e., docking against the "experimental" structure).

Discussion

Contrary to our expectations, the prospective large-library docking campaigns against the AF2 models were no less effective than those against experimental structures. The hit rates were high for both the σ_2 and 5-HT2A receptors across hundreds of molecules that we experimentally tested against each structure and were not significantly different between the AF2-modeled and the experimental structures. Comparing the affinities of these molecules yielded similar conclusions. Indeed, against the 5-HT2A receptor, the AF2 structure led, if anything, to more potent and selective compounds, with the mid-nM EC_{50} values of the docking hits ranking among the most potent and selective molecules to emerge from extensive structure-based campaigns (*61*) against this target. A cryo-EM structure of one of these new agonists, Z7757, largely confirmed the modeled prediction: The docking prediction superposed well with the position in the new cryo-EM structure (Fig. 5G), and even some of the key structural differences between the original AF2 model and the lisuride–5-HT2A cryo-EM

structure were recapitulated in the new cryo-EM structure of the Z7757–5-HT2A complex. These observations are consistent with the idea that the AF2 model captured low-energy, accessible states of the 5-HT2A receptor, even though those were not seen in the lisuride–5-HT2A cryo-EM structure used for docking in the "experimental structure" arm of the 5-HT2A receptor comparison.

These prospective results may be reconciled with previous retrospective studies that have suggested that experimental structures are superior to unrefined AF2 models for ligand discovery (*7*, *39*–*48*). In the previous work, known ligands were docked against experimental structures and AF2 models, and the former better enriched the knowns than did the AF2 models. This is also what we observed when we docked known ligands against the σ_2 and 5-HT2A receptors (fig. S2). However, retrospective campaigns are biased by past results and cannot necessarily predict prospective ones. Experimental structures are often determined with some of the known ligands, which typically fall into only a few broad chemotypes, and ligands discovered against one conformation of a protein might not rank as well against another low-energy conformation of that same protein. The prospective results reported here, where hundreds of topologically unrelated chemotypes were synthesized and experimentally tested in all four campaigns (two against the experimental structures, two against the AF2 models), support this idea. It is also supported by the low overlap, even at a scaffold level, between the active molecules found by the AF2 and the experimental docking campaigns (Figs. 2 and 3 and fig. S4). The conformations of the AF2 models are, for ligand recognition, meaningfully different from the experimental structures and prioritize not only different molecules but also different families of molecules. At least for a subset of targets, the different conformations sampled remain relevant to ligand discovery and may complement experimental structures for such purposes.

Certain caveats merit mentioning. We have focused on two targets where the AF2 conformations of the ligand binding sites are either quite close to that of the experimental structure, as for the σ_2 receptor, or are close with a few important divergences, as for the 5-HT2A receptor. There are other AF2 models that differ so much from the experimental structures that we deem them poor candidates for docking (fig. S1). We have not explored how many proteins fall into these different categories, nor is it entirely clear how one would know this a priori. The average binding site pLDDT (predicted local distance difference test) scores of MRGPRX4, which we deemed unsuitable for docking, for the 5-HT2A receptor and for the σ_2 receptors are 87, 95, and 95, respectively, suggesting that these scores might help rank AF2 structures that are better suited for ligand discovery. Also, the binding sites in both the experimental and the AF2 structures targeted for docking ranked as ligandable (*49*). Still, distinguishing between more and less suitable AF2 structures remains an active area of research. With respect to hit rates, although for binding these were high for both structures of both targets, the hit rates for functional ligands—agonists or antagonists—for the 5-HT2A receptor were low, in the 1 to 5% range. We suspect that this partly reflects our testing enantiomeric mixtures, because we have found that testing pure enantiomers can be crucial for detecting functional activity, as opposed to simple binding (*61*). Finally, The AF2 models used here were predicted without any ligand information. New tools like RoseTTAFold All-Atom (*78*) and the AlphaFold Latest (*79*) can cofold proteins with small molecules, potentially improving models for large-library docking.

These caveats should not obscure the central observations from this study. Although retrospective docking of known ligands against the AF2 models of the σ_2 and 5-HT2A receptors returned worse enrichment than did the experimental structures (fig. S2), when large libraries were docked prospectively against AF2 models, the hit rates were comparable to those returned by the experimental structures and were high in both cases. For both targets, the AF2 models prioritized different chemotypes than did the experimental structures. We speculate that the alternate conformations sampled by AF2 models capture low-energy conformations, which are useful for identifying ligands distinct from those recognized by the experimental structures. In the docking campaign against the 5-HT2A receptor, the functional profiles of hits derived from AF2 docking were no worse than those from experimental structure docking. Notably, three 5-HT2A receptor hits from docking against the AF2 model were subtype selective, something not seen in the campaign against the cryo-EM structure. Lastly, a cryo-EM structure for one of the AF2-derived agonists supported the docking prediction and, indeed, certain details of the AF2 modeled receptor conformation. We conclude that, under the right circumstances, AF2 models can expand the range of proteins targeted for structure-based discovery and the breadth of potent chemotypes discovered.

Materials and methods

Molecular docking against the experimental structure of the σ_2 and 5-HT2A receptors

The docking setups of the σ_2 and 5-HT2A campaigns were reported previously (*7*, *10*). The compound selection of the 5-HT2A campaign is described in the next subsection.

Molecular docking against the AF2 structure of the σ_2 and 5-HT2A receptors

The molecular docking procedures were conducted using the AF2 models of the σ_2 and 5-HT2A receptors, specifically the AF-Q5BJF2-F1-model_v1 for the σ_2 receptor and the AF-P28223-F1-model_v1 for the 5-HT2A receptor, both of which were downloaded from the AlphaFold Protein Structure Database (https://alphafold.ebi.ac.uk). The structures of both receptors were protonated at pH 7.0 using Epik and PROPKA in 2021-released Maestro. AMBER united atom charges were assigned to both structures. For the σ_2 receptor, E73 was modeled as a neutral residue. The receptor was embedded in a lipid bilayer to mimic its native environment in the endoplasmic reticulum membrane, followed by a 50-ns coarse-grained molecular dynamic (MD) simulation with a restricted receptor conformation. We note that this MD simulation was only used to define a lipid low-dielectric environment for the receptor, which was subsequently used in the calculation of the molecular electrostatic potential for the receptor; it did not change the coordinates of the AF2 model used in the docking, which were unrefined. The low dielectric and desolvation volumes were extended out 2.4 and 0.6 Å, respectively. For the 5-HT2A receptor, the low dielectric and desolvation volumes were extended out from the receptor surface by 2.0 and 0.6 Å, respectively. Energy grids for both receptors were pregenerated using CHEMGRID for AMBER van der Waals potential, QNIFFT for Poisson-Boltzmann–based electrostatic potentials, and SOLVMAP for ligand desolvation. The spheres generated by SPHGEN in the ligand binding site were used as matching spheres for docking known binders for each receptor against each apo AF2 model. Based on the predicted interactions from docking against apo AF2 models, the best docked pose of known binders for each receptor was then selected as matching spheres for the next steps. Twenty-seven spheres from the docked pose of PB28 were used for the σ_2 receptor. Eighteen spheres of lisuride were used for the 5-HT2A receptor. To speed up screening of 1.6 billion molecules for the 5-HT2A receptor, the 5-HT2A matching spheres were labeled according to charge-charge interaction and hydrogen-bond patterns and grouped into four clusters via k-means clustering for efficient searching in docking calculations.

The docking setups for both the σ_2 and 5-HT2A receptors were evaluated for their ability to enrich known ligands over property-matched decoys. The docking performance was evaluated using log-adjusted AUC values (logAUC). For the σ_2 receptor, the enrichment achieved a logAUC of 16 on the same ligand-decoy set used to evaluate the docking setup built from the experimental structure. We

used the same "extrema" set to ensure that molecules with extreme physical properties were not enriched. The docking setup enriched close to 80% monocations among the top 1000 ranking molecules. The logAUC was 36 using 10 σ_2 ligands against the "extrema" set. For the 5-HT2A receptor, this setup achieved a logAUC of 1.5 using the same ligand-decoy set as preparing the docking setup built from the cryo-EM structure. On the extrema test, the docking setup enriched more than 90% monocations among the top 1000 molecules, with a logAUC of 19. Additionally, a "goldilocks" set from the DUDE-Z web server was used to further test the setup, resulting in a logAUC of 10. The evaluation above confirmed the favorable docking parameters for both receptors for launching ultralarge-scale docking campaigns.

In the large-scale docking campaigns, 490 million cations from ZINC15 (http://zinc20.docking.org) were docked against the σ_2 receptor, and more than 1.6 billion library molecules from ZINC20/ZINC22 (http://zinc20.docking.org and https://cartblanche22.docking.org) were docked against the 5-HT2A receptor using DOCK3.8. On average, 2435 and 219 orientations were explored for the σ_2 and 5-HT2A receptors, respectively. On average, 180 and 340 conformations were sampled for the σ_2 and 5-HT2A receptors, respectively The total calculation times were 115,653 hours for the σ_2 receptor and 138,836 hours for the 5-HT2A receptors.

The σ_2 receptor AF2 campaign was processed by the same protocol used to process the docking campaign against the σ_2 receptor x-ray structure. The top-ranking 300,000 molecules were filtered for novelty using the ECFP4-based Tc against 2232 $\sigma_{1/2}$ ligands in ChEMBL (https://www.ebi.ac.uk/chembl/) and 574 σ_2 ligands from S2RSLDB (http://www.researchdsf.unict.it/S2RSLDB). Molecules with Tc ≥ 0.35 were eliminated. The remaining 213,805 molecules were filtered by three criteria: (i) total torsion strain energy of less than eight units, (ii) maximum strain energy per torsion angle of less than three units, and (iii) forms a salt bridge with D29. The last filter was implemented based on LUNA (https://github.com/keiserlab/LUNA). The remaining 57,662 molecules were clustered by the LUNA 1024-length binary fingerprint of a Tc = 0.32, resulting in 12,095 clusters. Ultimately, 81 compounds were chosen by human inspection and 24 consecutive ranked compounds were selected from three rankings: the 1st, 550th, and 3925th, the same machine picking ranks as the docking campaign against the x-ray structure. In total, 153 compounds were selected, 119 of which were successfully synthesized.

The 5-HT2A receptor campaigns against both experimental and AF2 structures were processed by the same protocol. The top-ranking 3.2 million molecules from both campaigns were filtered for novelty using the ECFP4-based Tc against 8601 5-HT2A, 5-HT2B, and 5-HT2C ligands in ChEMBL (https://www.ebi.ac.uk/chembl/). Molecules with Tc ≥ 0.35 were eliminated. The remaining top 2.67 million and 2.64 million molecules were filtered by interactions with D155, S242, S239, T160, S159, and F340 for experimental and AF2 campaigns, respectively. The interaction filters were implemented based on LUNA (https://github.com/keiserlab/LUNA). The remaining 4480 and 1452 molecules were clustered by the LUNA 1024-length binary fingerprint of a Tc = 0.35, resulting in 2298 and 828 clusters. Ultimately, 259 and 218 compounds were chosen by human inspection. Two hundred twenty-three and 161 compounds were successfully synthesized.

Make-on-demand synthesis

All the make-on-demand molecules were derived from the Enamine REAL database (https://enamine.net/compound-collections/real-compounds). See supplementary materials for synthesis procedure and characterization of compounds (supplementary methods and data S3).

Competition binding in Expi293 membranes

Membranes were prepared as previously described (7). Briefly, the human σ_2 receptor was cloned into pcDNA3.1 (Invitrogen) mammalian expression vector with an amino-terminal protein C tag followed by a 3C protease cleavage site and transfected into Expi293 cells (ThermoFisher Scientific) using FectoPRO (Polyplus-transfection) according to the manufacturer's instructions. Cells were harvested by centrifugation and lysed by osmotic shock in a buffer containing 20 mM HEPES, pH 7.5, 2 mM MgCl2, 1:100,000 (vol/vol) benzonase nuclease (Sigma Aldrich), and cOmplete Mini EDTA-free protease-inhibitor tablets (Sigma Aldrich). The lysates were homogenized with a glass Dounce tissue homogenizer and then centrifuged at 20,000*g* for 20 min. The pellet was resuspended in 50 mM Tris, pH 8.0; adjusted to 10 mg/ml; flash frozen in liquid nitrogen; and stored at −80°C until use.

Competition binding reactions were done in 100 μl, with 50 mM Tris pH 8.0, 10 nM [^{3}H]-DTG (PerkinElmer), and the indicated concentration of the competing ligand, and supplemented with 0.1% bovine serum albumin to minimize nonspecific binding. Samples were shaken at 37°C for 90 min. Afterward, the reaction was terminated by massive dilution and filtration over a glass microfiber filter with a Brandel harvester. Filters were soaked with 0.3% polyethyleneimine for at least 30 min before use. Radioactivity was measured by liquid scintillation counting. Data analysis was done in GraphPad Prism 9.0, with K_i values calculated by Cheng-Prusoff correction using the experimentally measured probe dissociation constant.

Radioligand binding assays

Competitive radioligand binding assays were conducted in the National Institute of Mental Health Psychoactive Drug Screening Program (NIMH PDSP) using 5-HT2A membranes prepared from transiently transfected human embryonic kidney (HEK) 293 cells in 96-well plates. Detailed assay protocols and conditions are also available from the NIMH PDSP homepage (https://pdsp.unc.edu/pdspweb/?site=assays)

Compounds [10 mM dimethyl sulfoxide (DMSO) stocks] were prepared in a standard binding buffer (50 mM Tris-HCl, pH 7.4, containing 10 mM $MgCl_2$ and 0.1 mM EDTA) supplemented with 1 mg/ml fatty acid–free bovine serum albumin and 0.1 mg/ml ascorbic acid. Samples were first screened at a single concentration of 10 μM with in-plate quadruplicate set (primary binding experiment). Those with a minimum of 90% inhibition at 10 μM were subjected to concentration response assays (12 points starting from 100 μM) to determine binding affinity (K_i) with in-plate duplicate set for three independent assays (secondary binding experiment). Radioligand [^{3}H]-LSD was used at the final concentration of 0.5 nM. To each well of a 96-well plate, containing 25 μl of the test compounds at 50 μM, 25 μl of the radioligand was added, followed by the addition of 75 μl of crude membrane fractions containing the 5-HT2A receptor in standard binding buffer. For primary binding experiments, nonspecific binding was determined in the presence of 10 μM clozapine. The reaction mixture was incubated at room temperature for 2 hours. Receptor-bound radioactivity was harvested by rapid filtration onto UniFilter-96 GF/C Microplates (PerkinElmer) using a Filtermate harvester (PerkinElmer). The dried plates were treated with MicroScint-O liquid scintillation cocktails (PerkinElmer), and the captured radioactivity was measured using a MicroBeta scintillation counter. Concentration response inhibition results were analyzed using the "Binding Competitive – One site Fit Ki" model in GraphPad Prism version 10.1.0 (GraphPad Prism).

Calcium mobilization assay

Calcium mobilization was measured using Fluo-4 Direct calcium dye (Invitrogen). To measure calcium mobilization for 5-HT2A, 5-HT2B, and 5-HT2C, HEK293 cell lines stably transfected with each individual receptor were maintained in Dulbecco's modified Eagle's media (DMEM) supplemented with 10% fetal bovine serum (FBS), 100 IU/ml penicillin, 100 mg/ml streptomycin, 100 μg/ml hygromycin B, and 15 μg/ml blasticidin in a humidified incubator at 37°C and 5% CO_2. To induce receptor expression, 5-HT2A, 5-HT2B, and 5-HT2C stable cells were treated with 1.5 μg/ml tetracycline and seeded into 384-well black plates in DMEM supplemented with 1% dialyzed FBS

(dFBS), 100 IU/ml penicillin, and 100 mg/ml streptomycin at a cell density of ~15,000 cells per well. To measure calcium mobilization for the V1A vasopressin receptor, CHO cells stably transfected with the receptor were maintained in Ham's F-12 media supplemented with 10% FBS, 100 IU/ml penicillin, 100 mg/ml streptomycin, and 400 μg/ml G418 in a humidified incubator at 37°C and 5% CO_2. V1A stable cells were seeded into 384-well black plates in Ham's F-12 media supplemented with 1% dFBS, 100 IU/ml penicillin, and 100 mg/ml streptomycin at a cell density of ~8000 cells per well.

Twenty-four hours later, cells were incubated with 20 μl Fluo-4 Direct calcium dye (Invitrogen) supplemented with 2 mM probenecid (ThermoFisher) in drug buffer [1X HBSS, 20 mM HEPES, 0.1% (w/v) BSA, 0.01% (w/v) ascorbic acid, pH 7.4] for 1 hour at 37°C and 5% CO_2, then 20 min at room temperature in the dark. All drug dilutions were prepared at a 3X concentration in drug buffer for screening (3 μM or 1μM final concentration for serotonin or V1A vasopressin receptor screens, respectively) or dose-response profiling (16-point titration) and transferred into a 384-well drug plate. Calcium flux was quantified using a FLIPRPENTA fluorescence imaging plate reader (Molecular Dynamics) by first measuring baseline for 10 s (1 read/s), then after addition of 10 μl 3X drug for 120 s (1 read/s). For antagonist data, 10 μl agonist (10 nM 5-HT or 100 nM vasopressin) was added 15 min after drug treatment to stimulate calcium mobilization. Maximal raw fluorescence values over the 120-s experiment were transformed to fold-change relative to baseline fluorescence (mean of the first 10 reads before drug addition) and plotted for each dose to generate endpoint screening data or dose-response curves. These data were normalized relative to serotonin or vasopressin (agonist control), clozapine (5-HT2A, 5-HT2B, and 5-HT2C antagonist control), or vehicle (baseline for V1A antagonist screen) and plotted as bar graphs (screening data) or fit using the "log (agonist) versus response (three parameter)" or "log (inhibitor) versus response (three parameter)" functions in GraphPad Prism version 10.1.0 (GraphPad Software). An activity threshold of 10% maximal agonist response or 80% maximal response after agonist stimulation (10 nM 5-HT or 100 nM vasopressin in antagonist mode) was used to identify compounds that exhibit agonist or antagonist activity, respectively. Importantly, dose-response curves for compounds with agonist activity (≥10% maximal agonist response at 10 μM) at a given receptor were removed from antagonist mode plots.

BRET assays

BRET assays were performed to measure $G\alpha_q$ protein dissociation (BRET2) and β-arr2 recruitment (BRET1) as described previously (*2*, *72*). For $G\alpha_q$ protein-dissociation measurements, wild-type 5-HT2A, 5-HT2B, and 5-HT2C were cotransfected with $G\alpha_q$-RLuc8, $G_{\beta 3}$, and GFP2- $G_{\gamma 9}$ in a 1:1:1:1 ratio in HEK293 cells maintained in DMEM supplemented with 10% FBS and 1% penicillin-streptomycin (pen-strep). After 12 hours, cells were plated in 96-well microplates in DMEM supplemented with 1% dFBS and 1% pen-strep. After 12 hours of plating the cells, media was vacuum aspirated and followed by addition of 60 μl of assay buffer (1X Hank's balanced salt solution in phosphate buffered saline, 20 mM HEPES, pH 7.4) into the wells, and plates were incubated at 37°C for 10 min. After that, 30 μl of 3X drug diluted in drug buffer (assay buffer supplemented with 0.1% fatty acid–free bovine serum albumin and 0.01% ascorbic acid) were added to the wells. Plates were incubated at 37°C for 10 min. Plates were then removed and kept at room temperature for another 10 min followed by the addition of 10 μl of coelenterazine 400a diluted in assay buffer at a concentration of 50 μM. Plates were incubated for another 10 min at room temperature and then read using a BMG Labtech PHERAstar FSX with BRET2 plus optic module. For BRET1, RLuc8 was cloned directly to the C terminus of wild-type 5-HT2A, 5-HT2B, and 5-HT2C, and experiments were performed as described previously (*2*). HEK293T cells were cotransfected with receptor, GRK2, and mVenus-β-arr2 in a 1:1:5 ratio. BRET1 measurements were done identically to those for BRET2, though coelenterazine h was used instead of coelenterazine 400a. Plates were read using a BMG Labtech PHERAstar FSX with BRET1 plus optic module. All data were analyzed using GraphPad Prism 9.0.

DLS

Samples were prepared in filtered 50 mM KPi buffer, pH 7.0, with a final DMSO concentration at 1% (v/v). Colloidal particle formation was measured using either a DynaPro Plate Reader II or a DynaPro MS/X (both Wyatt Technology). All compounds were screened in triplicate at 31.6 μM. Colloidal particles were defined as having a scattering intensity of at least one order of magnitude greater than background scattering and a hydrodynamic radius greater than 100 nm in size (*80*). All data were analyzed using GraphPad Prism software version 9.1.1 (San Diego, CA).

MDH enzyme inhibition assays

Enzyme inhibition assays were performed at room temperature using CLARIOstar Plate Reader (BMG Labtech). Samples were prepared in 50 mM KPi buffer, pH 7.0, with a final DMSO concentration at 1% (v/v). Compounds were incubated with 2 nM MDH for 5 min. Reactions were initiated by the addition of 200 μM nicotinamide adenine dinucleotide (NADH) (54839, Sigma Aldrich) and 200 μM oxaloacetic acid (324427, Sigma Aldrich). The change in absorbance was monitored at 340 nm for 1 min 20 s. Initial rates were divided by the DMSO control rate to determine enzyme activity (%). Each compound was initially screened at 31.6 μM in triplicate. Data were analyzed using GraphPad Prism software version 9.1.1 (San Diego, CA).

Protein purification

Protein purification and complex formation were carried out as previously described (*60*, *67*, *76*). After expression in *Spodoptera frugiperda* (Sf9) the 5-HT2A receptor (with the respective ligand), mini-Gαq, and scFv16 were purified as previously described. In the case of the lisuride complex, each of the components was mixed in a 1:1.2:1.5 molar equivalent ratio of receptor: mini-Gαq:scFv16 and allowed to incubate overnight at 4°C. The mixture was further purified by Superdex 200 10/300 column in 20 mM HEPES (pH 7.5), 100 mM NaCl, 0.001% (w/v) lauryl maltose neopentyl glycol (LMNG), 0.0001% (w/v) cholesterol hemisuccinate (CHS), 0.00025% (w/v) glyco-diosgenin (GDN), 100 μM tris(2-carboxyethyl)phosphine (TCEP), and 50 μM lisuride. For the Z7757 structure, the 5-HT2A receptor and mini-Gαq heterotrimer were co-expressed using a multiplicity of infection (MOI) of 3:1.5. Isolation of the complex was carried out in the same way as the receptor purification, with the addition of 500 μg of scFv16 during membrane solubilization. The first round of size exclusion was carried out in 20 mM HEPES (pH 7.5), 100 mM NaCl, 0.001% (w/v) LMNG, 0.0001% (w/v) CHS, 0.00025% (w/v) GDN, 100 μM TCEP, and 50 μM Z7757 on a Superose 6 column, and peak fractions corresponding to the complex were collected. Each sample was concentrated to 3 mg/ml for the Z7757 sample or 15 mg/ml for the lisuride sample before preparing grids.

cryo-EM data collection and processing

Grids were prepared by applying 3.5 μl of the Z7757 complex or 2 μl of the lisuride complex to glow discharged UltrAuFoil holey gold grids (Quantifoil, Au300-R1.2/1.3). The girds containing Z7757 were then vitrified by plunge freezing into a 60/40 mixure of liquid ethane/propane using a Vitrobot mark IV (FEI) set at 22°C and 100% humidity, whereas the grids containing lisuride were vitrified by plunge freezing into liquid ethane at 18°C and 100% humidity. Movies were then collected on a Titan Krios operated at 300 keV with a K3 Summit direct electron detector (Gatan) at a magnification of 57,050×. A total of 5095 movies were collected with 50 frames per movie over a total dose of 50 electrons/$Å^2$ and a defocus range of 0.5 to 2.5 μm for Z7757. For the lisuride complex, a total of 3282 movies were collected, dose-fractionated over 50 frames, and recorded

for 0.05 s per frame, resulting in a total dose of 67.78 electrons/Å^2 in super-resolution mode with a defocus range of 0.8 to 1.8 μm. The data processing tree for the Z7757 dataset can be found in fig. S14. In short, motion correction and contrast transfer function (CTF) estimation were done using cryoSPARC (*81*) and initial sets of particle picking, 2D classification, initial models, and 3D refinement. A set of approximately 554,537 particles were then carried over into Relion (*82*) for multiple rounds of no-alignment 3D classification focused on the TM domain. Subsequent rounds of NU-Refine (carried out in cryoSPARC) and Bayesian polishing (carried out in Relion) were then performed. Once a good consensus map was achieved from NU-refine, subsequent local refinement with a soft mask was carried out for both the receptor and heterotrimer in cryoSPARC, which were then combined for a consensus reconstruction. For the lisuride complex, the processing tree can be found in fig. S5. In short, the data processing was done in cryoSPARC with a total of 2,426,824 particles extracted from the corrected micrographs. After 2D and 3D classification, a subset of 133,216 particles underwent homogeneous refinement, followed by local refinements of the lisuride-bound receptor and the heterotrimeric miniGq (bound to the active-state stabilizing single-chain variable fragment, scFv16) at resolutions of 3.1 and 2.8 Å, respectively. Maps resulting from local refinements were combined in Chimera to produce the final reconstruction.

Model building and refinement

The initial model was fit using nonclassical agonist *R*-69 (PDB ID 7RAN) (*61*). All models were docked into the cryo-EM density using either Chimera (*83*) or ChimeraX (*84*). Subsequent real-space refinement was carried out in Phenix (*85*), and iterative manual fitting and adjustments were carried out with COOT (*86*). The binding pose was further validated by using Emerald for Z7757 and the Gemspot pipeline for lisuride (*63*, *77*). Final model statistics were validated by Molprobity (*87*) (table S2). All structural figures were visualized in either Chimera (*83*) or ChimeraX (*84*).

REFERENCES AND NOTES

1. A. V. Sadybekov, V. Katritch, Computational approaches streamlining drug discovery. *Nature* **616**, 673–685 (2023). doi: 10.1038/s41586-023-05905-z; pmid: 37100941
2. Y. Wang *et al*., Structures of the entire human opioid receptor family. *Cell* **186**, 413–427.e17 (2023). doi: 10.1016/j.cell.2022.12.026; pmid: 36638794
3. P. Xu *et al*., Structural insights into the lipid and ligand regulation of serotonin receptors. *Nature* **592**, 469–473 (2021). doi: 10.1038/s41586-021-03376-8; pmid: 33762731
4. J. Lyu *et al*., Ultra-large library docking for discovering new chemotypes. *Nature* **566**, 224–229 (2019). doi: 10.1038/s41586-019-0917-9; pmid: 30728502
5. R. M. Stein *et al*., Virtual discovery of melatonin receptor ligands to modulate circadian rhythms. *Nature* **579**, 609–614 (2020). doi: 10.1038/s41586-020-2027-0; pmid: 32040955
6. C. Gorgulla *et al*., An open-source drug discovery platform enables ultra-large virtual screens. *Nature* **580**, 663–668 (2020). doi: 10.1038/s41586-020-2117-z; pmid: 32152607
7. A. Alon *et al*., Structures of the σ_2 receptor enable docking for bioactive ligand discovery. *Nature* **600**, 759–764 (2021). doi: 10.1038/s41586-021-04175-x; pmid: 34880501
8. E. A. Fink *et al*., Structure-based discovery of nonopioid analgesics acting through the α_{2A}-adrenergic receptor. *Science* **377**, eabn7065 (2022). doi: 10.1126/science.abn7065; pmid: 36173843
9. A. A. Sadybekov *et al*., Synthon-based ligand discovery in virtual libraries of over 11 billion compounds. *Nature* **601**, 452–459 (2022). doi: 10.1038/s41586-021-04220-9; pmid: 34912117
10. J. Lyu, J. J. Irwin, B. K. Shoichet, Modeling the expansion of virtual screening libraries. *Nat. Chem. Biol.* **19**, 712–718 (2023). doi: 10.1038/s41589-022-01234-w; pmid: 36646956
11. A. Manglik *et al*., Structure-based discovery of opioid analgesics with reduced side effects. *Nature* **537**, 185–190 (2016). doi: 10.1038/nature19112; pmid: 27533032
12. J. Reis *et al*., Targeting ROS production through inhibition of NADPH oxidases. *Nat. Chem. Biol.* **19**, 1540–1550 (2023). doi: 10.1038/s41589-023-01457-5; pmid: 37884805
13. C. Gorgulla *et al*., VirtualFlow 2.0-The next generation drug discovery platform enabling adaptive screens of 69 billion molecules. bioRxiv 2023.2004.2025.537981 [Preprint] (2023); https://doi.org/10.1101/2023.04.25.537981.
14. A. S. Hauser *et al*., Pharmacogenomics of GPCR drug targets. *Cell* **172**, 41–54.e19 (2018). doi: 10.1016/j.cell.2017.11.033; pmid: 29249361
15. J. Carlsson *et al*., Ligand discovery from a dopamine D3 receptor homology model and crystal structure. *Nat. Chem. Biol.* **7**, 769–778 (2011). doi: 10.1038/nchembio.662; pmid: 21926995
16. T. Beuming, W. Sherman, Current assessment of docking into GPCR crystal structures and homology models: Successes, challenges, and guidelines. *J. Chem. Inf. Model.* **52**, 3263–3277 (2012). doi: 10.1021/ci300411b; pmid: 23121495
17. A. Hillisch, L. F. Pineda, R. Hilgenfeld, Utility of homology models in the drug discovery process. *Drug Discov. Today* **9**, 659–669 (2004). doi: 10.1016/S1359-6446(04)03196-4; pmid: 15279849
18. A. Bordogna, A. Pandini, L. Bonati, Predicting the accuracy of protein-ligand docking on homology models. *J. Comput. Chem.* **32**, 81–98 (2011). doi: 10.1002/jcc.21601; pmid: 20607693
19. J. Jumper *et al*., Highly accurate protein structure prediction with AlphaFold. *Nature* **596**, 583–589 (2021). doi: 10.1038/s41586-021-03819-2; pmid: 34265844
20. M. Baek *et al*., Accurate prediction of protein structures and interactions using a three-track neural network. *Science* **373**, 871–876 (2021). doi: 10.1126/science.abj8754; pmid: 34282049
21. M. Varadi *et al*., AlphaFold Protein Structure Database: Massively expanding the structural coverage of protein-sequence space with high-accuracy models. *Nucleic Acids Res.* **50**, D439–D444 (2022). doi: 10.1093/nar/gkab1061; pmid: 34791371
22. K. Tunyasuvunakool *et al*., Highly accurate protein structure prediction for the human proteome. *Nature* **596**, 590–596 (2021). doi: 10.1038/s41586-021-03828-1; pmid: 34293799
23. S. Hutin *et al*., The Vaccinia virus DNA helicase structure from combined single-particle cryo-electron microscopy and AlphaFold2 prediction. *Viruses* **14**, 2206 (2022). doi: 10.3390/v14102206; pmid: 36298761
24. S. Mosalaganti *et al*., AI-based structure prediction empowers integrative structural analysis of human nuclear pores. *Science* **376**, eabm9506 (2022). doi: 10.1126/science.abm9506; pmid: 35679397
25. M. Akdel *et al*., A structural biology community assessment of AlphaFold2 applications. *Nat. Struct. Mol. Biol.* **29**, 1056–1067 (2022). doi: 10.1038/s41594-022-00849-w; pmid: 36344848
26. M. Jendrusch, J. O. Korbel, S. K. Sadiq, AlphaDesign: A de novo protein design framework based on AlphaFold. bioRxiv 2021.2010.2011.463937 [Preprint] (2021); https://doi.org/10.1101/2021.10.11.463937.
27. C. A. Goverde, B. Wolf, H. Khakzad, S. Rosset, B. E. Correia, De novo protein design by inversion of the AlphaFold structure prediction network. *Protein Sci.* **32**, e4653 (2023). doi: 10.1002/pro.4653; pmid: 37165539
28. P. Bryant, G. Pozzati, A. Elofsson, Improved prediction of protein-protein interactions using AlphaFold2. *Nat. Commun.* **13**, 1265 (2022). doi: 10.1038/s41467-022-28865-w; pmid: 35273146
29. R. Yin, B. Y. Feng, A. Varshney, B. G. Pierce, Benchmarking AlphaFold for protein complex modeling reveals accuracy determinants. *Protein Sci.* **31**, e4379 (2022). doi: 10.1002/pro.4379; pmid: 35900023
30. R. Evans *et al*., Protein complex prediction with AlphaFold-Multimer. bioRxiv 2021.2010.2004.463034 [Preprint] (2021); https://doi.org/10.1101/2021.10.04.463034.
31. S. Wang *et al*., CavitySpace: A database of potential ligand binding sites in the human proteome. *Biomolecules* **12**, 967 (2022). doi: 10.3390/biom12070967; pmid: 35883523
32. M. van Kempen *et al*., Fast and accurate protein structure search with Foldseek. *Nat. Biotechnol.* **42**, 243–246 (2024). doi: 10.1038/s41587-023-01773-0; pmid: 37156916
33. W. Ma *et al*., Enhancing protein function prediction performance by utilizing AlphaFold-predicted protein structures. *J. Chem. Inf. Model.* **62**, 4008–4017 (2022). doi: 10.1021/acs.jcim.2c00885; pmid: 36006049
34. M. L. Hekkelman, I. de Vries, R. P. Joosten, A. Perrakis, AlphaFill: Enriching AlphaFold models with ligands and cofactors. *Nat. Methods* **20**, 205–213 (2023). doi: 10.1038/s41592-022-01685-y; pmid: 36424442
35. M. C. Weghoff, J. Bertsch, V. Müller, A novel mode of lactate metabolism in strictly anaerobic bacteria. *Environ. Microbiol.* **17**, 670–677 (2015). doi: 10.1111/1462-2920.12493; pmid: 24762045
36. S. Kimura *et al*., Sequential action of a tRNA base editor in conversion of cytidine to pseudouridine. *Nat. Commun.* **13**, 5994 (2022). doi: 10.1038/s41467-022-33714-x; pmid: 36220828
37. H. Tao *et al*., Discovery of non-squalene triterpenes. *Nature* **606**, 414–419 (2022). doi: 10.1038/s41586-022-04773-3; pmid: 35650436
38. J. M. Thornton, R. A. Laskowski, N. Borkakoti, AlphaFold heralds a data-driven revolution in biology and medicine. *Nat. Med.* **27**, 1666–1669 (2021). doi: 10.1038/s41591-021-01533-0; pmid: 34642488
39. M. Holcomb, Y.-T. Chang, D. S. Goodsell, S. Forli, Evaluation of AlphaFold2 Structures as Docking Targets. *Protein Sci.* **32**, e4530 (2022). doi: 10.1002/pro.4530; pmid: 9794023
40. M. Karelina, J. J. Noh, R. O. Dror, How accurately can one predict drug binding modes using AlphaFold models? *eLife* **12**, e89386.1 (2023). doi: 10.7554/eLife.89386.1; pmid: 35778488
41. X. He *et al*., AlphaFold2 versus experimental structures: Evaluation on G protein-coupled receptors. *Acta Pharmacol. Sin.* (2022). doi: 10.1038/s41401-022-00938-y; pmid: 35778488
42. V. Scardino, J. I. Di Filippo, C. N. Cavasotto, How good are AlphaFold models for docking-based virtual screening? *iScience* **26**, 105920 (2022). doi: 10.1016/j.isci.2022.105920; pmid: 36686396
43. A. M. Díaz-Rovira *et al*., Are deep learning structural models sufficiently accurate for virtual screening? Application of docking algorithms to AlphaFold2 predicted structures. *J. Chem. Inf. Model.* **63**, 1668–1674 (2023). doi: 10.1021/acs.jcim.2c01270; pmid: 36892986
44. F. Wong *et al*., Benchmarking AlphaFold-enabled molecular docking predictions for antibiotic discovery. *Mol. Syst. Biol.* **18**, e11081 (2022). doi: 10.15252/msb.202211081; pmid: 36065847
45. Y. Zhang *et al*., Benchmarking refined and unrefined AlphaFold2 structures for hit discovery. *J. Chem. Inf. Model.* **63**, 1656–1667 (2023). doi: 10.1021/acs.jcim.2c01219; pmid: 36897766
46. T. Beuming *et al*., Are deep learning structural models sufficiently accurate for free-energy calculations? Application of FEP+ to AlphaFold2-predicted structures. *J. Chem. Inf. Model.* **62**, 4351–4360 (2022). doi: 10.1021/acs.jcim.2c00796; pmid: 36099477
47. M. Karelina, J. J. Noh, R. O. Dror, How accurately can one predict drug binding modes using AlphaFold models? *eLife* **12**, e89386 (2023). doi: 10.7554/eLife.89386; pmid: 38131311
48. D. Lowe, "Docking with AlphaFold structures: Oops," *In the Pipeline* (blog), *Science*, 24 August 2023.
49. T. A. Halgren, Identifying and characterizing binding sites and assessing druggability. *J. Chem. Inf. Model.* **49**, 377–389 (2009). doi: 10.1021/ci800324m; pmid: 19434839
50. M. M. Mysinger, B. K. Shoichet, Rapid context-dependent ligand desolvation in molecular docking. *J. Chem. Inf. Model.* **50**, 1561–1573 (2010). doi: 10.1021/ci100214a; pmid: 20735049
51. R. G. Coleman, M. Carchia, T. Sterling, J. J. Irwin, B. K. Shoichet, Ligand pose and orientational sampling in

molecular docking. *PLOS ONE* **8**, e75992 (2013). doi: 10.1371/journal.pone.0075992; pmid: 24098414
52. E. C. Meng, B. K. Shoichet, I. D. Kuntz, Automated docking with grid-based energy evaluation. *J. Comput. Chem.* **13**, 505–524 (1992). doi: 10.1002/jcc.540130412
53. B. K. Shoichet, A. R. Leach, I. D. Kuntz, Ligand solvation in molecular docking. *Proteins* **34**, 4–16 (1999). doi: 10.1002/(SICI)1097-0134(19990101)34:1<4::AID-PROT2>3.0.CO;2-6; pmid: 10336382
54. S. Gu, M. S. Smith, Y. Yang, J. J. Irwin, B. K. Shoichet, Ligand strain energy in large library docking. *J. Chem. Inf. Model.* **61**, 4331–4341 (2021). doi: 10.1021/acs.jcim.1c00368; pmid: 34467754
55. R. A. Friesner *et al.*, Glide: A new approach for rapid, accurate docking and scoring. 1. Method and assessment of docking accuracy. *J. Med. Chem.* **47**, 1739–1749 (2004). doi: 10.1021/jm0306430; pmid: 15027865
56. T. A. Halgren *et al.*, Glide: A new approach for rapid, accurate docking and scoring. 2. Enrichment factors in database screening. *J. Med. Chem.* **47**, 1750–1759 (2004). doi: 10.1021/jm030644s; pmid: 15027866
57. R. Abagyan, M. Totrov, D. Kuznetsov, ICM—A new method for protein modeling and design: Applications to docking and structure prediction from the distorted native conformation. *J. Comput. Chem.* **15**, 488–506 (1994). doi: 10.1002/jcc.540150503
58. O. Trott, A. J. Olson, AutoDock Vina: Improving the speed and accuracy of docking with a new scoring function, efficient optimization, and multithreading. *J. Comput. Chem.* **31**, 455–461 (2010). doi: 10.1002/jcc.21334; pmid: 19499576
59. J. J. Irwin *et al.*, ZINC20—A free ultralarge-scale chemical database for ligand discovery. *J. Chem. Inf. Model.* **60**, 6065–6073 (2020). doi: 10.1021/acs.jcim.0c00675; pmid: 33118813
60. K. Kim *et al.*, Structure of a hallucinogen-activated Gq-coupled 5-HT_{2A} serotonin receptor. *Cell* **182**, 1574–1588.e19 (2020). doi: 10.1016/j.cell.2020.08.024; pmid: 32946782
61. A. L. Kaplan *et al.*, Bespoke library docking for 5-HT_{2A} receptor agonists with antidepressant activity. *Nature* **610**, 582–591 (2022). doi: 10.1038/s41586-022-05258-z; pmid: 36171289
62. A. Koehl *et al.*, Structure of the μ-opioid receptor-G_i protein complex. *Nature* **558**, 547–552 (2018). doi: 10.1038/s41586-018-0219-7; pmid: 29899455
63. M. J. Robertson, G. C. P. van Zundert, K. Borrelli, G. Skiniotis, GemSpot: A pipeline for robust modeling of ligands into cryo-EM maps. *Structure* **28**, 707–716.e3 (2020). doi: 10.1016/j.str.2020.04.018; pmid: 32413291
64. R. Xia *et al.*, Cryo-EM structure of the human histamine H_1 receptor/G_q complex. *Nat. Commun.* **12**, 2086 (2021). doi: 10.1038/s41467-021-22427-2; pmid: 33828102
65. J. I. Mobbs *et al.*, Structures of the human cholecystokinin 1 (CCK1) receptor bound to Gs and Gq mimetic proteins provide insight into mechanisms of G protein selectivity. *PLOS Biol.* **19**, e3001295 (2021). doi: 10.1371/journal.pbio.3001295; pmid: 34086670
66. C. Cao *et al.*, Signaling snapshots of a serotonin receptor activated by the prototypical psychedelic LSD. *Neuron* **110**, 3154–3167.e7 (2022). doi: 10.1016/j.neuron.2022.08.006; pmid: 36087581
67. R. H. Gumpper, J. F. Fay, B. L. Roth, Molecular insights into the regulation of constitutive activity by RNA editing of 5HT_{2C} serotonin receptors. *Cell Rep.* **40**, 111211 (2022). doi: 10.1016/j.celrep.2022.111211; pmid: 35977511
68. D. Cao *et al.*, Structure-based discovery of nonhallucinogenic psychedelic analogs. *Science* **375**, 403–411 (2022). doi: 10.1126/science.abl8615; pmid: 35084960
69. G. Pándy-Szekeres *et al.*, GPCRdb in 2023: State-specific structure models using AlphaFold2 and new ligand resources. *Nucleic Acids Res.* **51**, D395–D402 (2023). doi: 10.1093/nar/gkac1013; pmid: 36395823
70. V. Isberg *et al.*, Generic GPCR residue numbers - aligning topology maps while minding the gaps. *Trends Pharmacol. Sci.* **36**, 22–31 (2015). doi: 10.1016/j.tips.2014.11.001; pmid: 25541108
71. I. A. Simon *et al.*, Ligand selectivity hotspots in serotonin GPCRs. *Trends Pharmacol. Sci.* **44**, 978–990 (2023). doi: 10.1016/j.tips.2023.09.012; pmid: 37914598
72. R. H. J. Olsen *et al.*, TRUPATH, an open-source biosensor platform for interrogating the GPCR transducerome. *Nat. Chem. Biol.* **16**, 841–849 (2020). doi: 10.1038/s41589-020-0535-8; pmid: 32367019
73. B. K. Shoichet, Interpreting steep dose-response curves in early inhibitor discovery. *J. Med. Chem.* **49**, 7274–7277 (2006). doi: 10.1021/jm061103g; pmid: 17149857
74. M. F. Sassano, A. K. Doak, B. L. Roth, B. K. Shoichet, Colloidal aggregation causes inhibition of G protein-coupled receptors. *J. Med. Chem.* **56**, 2406–2414 (2013). doi: 10.1021/jm301749y; pmid: 23437772
75. Y. Liu *et al.*, Ligand recognition and allosteric modulation of the human MRGPRX1 receptor. *Nat. Chem. Biol.* **19**, 416–422 (2023). doi: 10.1038/s41589-022-01173-6; pmid: 36302898
76. C. Cao *et al.*, Structure, function and pharmacology of human itch GPCRs. *Nature* **600**, 170–175 (2021). doi: 10.1038/s41586-021-04126-6; pmid: 34789874
77. A. Muenks, S. Zepeda, G. Zhou, D. Veesler, F. DiMaio, Automatic and accurate ligand structure determination guided by cryo-electron microscopy maps. *Nat. Commun.* **14**, 1164 (2023). doi: 10.1038/s41467-023-36732-5; pmid: 36859493
78. R. Krishna *et al.*, Generalized biomolecular modeling and design with RoseTTAFold All-Atom. *Science* **384**, eadl2528 (2024). doi: 10.1126/science.adl2528; pmid: 38452047
79. Google DeepMind AlphaFold Team, Isomorphic Labs Team, "Performance and structural coverage of the latest, in-development AlphaFold model" (2023).
80. A. N. Ganesh, E. N. Donders, B. K. Shoichet, M. S. Shoichet, Colloidal aggregation: From screening nuisance to formulation nuance. *Nano Today* **19**, 188–200 (2018). doi: 10.1016/j.nantod.2018.02.011; pmid: 30250495
81. A. Punjani, J. L. Rubinstein, D. J. Fleet, M. A. Brubaker, cryoSPARC: Algorithms for rapid unsupervised cryo-EM structure determination. *Nat. Methods* **14**, 290–296 (2017). doi: 10.1038/nmeth.4169; pmid: 28165473
82. S. H. Scheres, RELION: Implementation of a Bayesian approach to cryo-EM structure determination. *J. Struct. Biol.* **180**, 519–530 (2012). doi: 10.1016/j.jsb.2012.09.006; pmid: 23000701
83. E. F. Pettersen *et al.*, UCSF Chimera—A visualization system for exploratory research and analysis. *J. Comput. Chem.* **25**, 1605–1612 (2004). doi: 10.1002/jcc.20084; pmid: 15264254
84. E. F. Pettersen *et al.*, UCSF ChimeraX: Structure visualization for researchers, educators, and developers. *Protein Sci.* **30**, 70–82 (2021). doi: 10.1002/pro.3943; pmid: 32881101
85. D. Liebschner *et al.*, Macromolecular structure determination using x-rays, neutrons and electrons: Recent developments in Phenix. *Acta Crystallogr. D Struct. Biol.* **75**, 861–877 (2019). doi: 10.1107/S2059798319011471; pmid: 31588918
86. P. Emsley, B. Lohkamp, W. G. Scott, K. Cowtan, Features and development of Coot. *Acta Crystallogr. D Biol. Crystallogr.* **66**, 486–501 (2010). doi: 10.1107/S0907444910007493; pmid: 20383002
87. V. B. Chen *et al.*, MolProbity: All-atom structure validation for macromolecular crystallography. *Acta Crystallogr. D Biol. Crystallogr.* **66**, 12–21 (2010). doi: 10.1107/S0907444909042073; pmid: 20057044
88. J. Lyu *et al.*, The docked poses from the docking screens against the AlphaFold2 models of the σ2 and 5HT2A receptors. Dryad (2024); https://doi.org/10.5061/dryad.sbcc2frf5.

ACKNOWLEDGMENTS

We thank OpenEye Software for the use of Omega and Schrodinger LLC for the use of the prepwizard and SiteMap programs in Maestro; all programs are available to the community from these companies. **Funding:** Funding for this work was provided by NIH grants R35GM122481 (to B.K.S.), GM133836 (to J.J.I.), and RO1MH112205, R37DA045657, and RO1GM119185 (to B.L.R.); by Defense Advanced Research Projects Agency (DARPA) grant HR00112020029 (to B.L.R.); and by the Vallee Foundation and the Sanofi iAwards program (to A.C.K.). **Author contributions:** J.L., B.K.S., A.C.K., and B.L.R. conceived the study. J.L. conducted the docking, chemoinformatics analyses, and ligand picking; T.A.T., S.H., and B.K.S. assisted with the latter. N.K., M.K.J., K.S., Y.K., J.D., and B.L.R. performed the 5-HT2A, 5-HT2B, and 5-HT2C receptor assays and analysis. R.G., L.W., X.B.-Á., K.K., G.S., and B.L.R. determined the cryo-EM 5-HT2A structures. A.A. and A.C.K. performed the σ_2 receptor assays and analysis. I.S.G. performed the aggregation assays. O.O.T. and Y.M. supervised the synthesis of molecules from the virtual library. J.J.I. was responsible for building the version of the ZINC library that was docked. A.C.K., B.K.S., and B.L.R. supervised the project. The manuscript was written by J.L., B.K.S., N.K., R.G., and B.L.R. with input from the other authors. **Competing interests:** B.K.S. is co-founder of BlueDolphin LLC, Epiodyne, and Deep Apple Therapeutics, Inc.; serves on the scientific review boards of Genentech, Schrodinger LLC, and Vilya Therapeutics; and consults for Levator Therapeutics, Hyku Therapeutics, and Great Point Ventures. J.J.I. co-founded Deep Apple Therapeutics, Inc., and BlueDolphin LLC. B.L.R is a co-founder of Epiodyne and Onsero and is on the scientific advisory boards of Onsero, Epiodyne, Levator, Escient, and Septerna. A.C.K. is a co-founder and consultant for biotechnology companies Tectonic Therapeutic and Seismic Therapeutic and for the Institute for Protein Innovation, a nonprofit research institute; A.C.K. is also a member of the board of directors of Tectonic Therapeutic. X.B.-Á. is now a senior scientist at Tectonic Therapeutics. **Data and materials availability:** The compounds docked in this study are freely available from our ZINC20 and ZINC22 databases at http://zinc20.docking.org and https://cartblanche22.docking.org, respectively. The cryo-EM density map and corresponding coordinates have been deposited in the Electron Microscopy Data Bank (EMDB) and the PDB under accession codes EMD-42676 and PDB ID 8UWL (5-HT2AR/miniGq/lisuride) and EMD-42999 and PDB ID 8V6U (5-HT2AR/miniGq/Z77575). Coordinates of characteristic docking-predicted ligand-receptor structures have been deposited in Dryad (*88*). DOCK3.8 is freely available for noncommercial research http://dock.compbio.ucsf.edu/DOCK3.8/. A web-based version available to all can be found at https://blaster.docking.org/.

SUPPLEMENTARY MATERIALS

science.org/doi/10.1126/science.adn6354
Figs. S1 to S16
Tables S1 to S6
MDAR Reproducibility Checklist
Data S1 to S5

Submitted 19 December 2023; accepted 24 April 2024
Published online 16 May 2024
10.1126/science.adn6354